Fully coupled atmosphere-hydrology simulations for the central Mediterranean: Impact of enhanced hydrological parameterization for short and long time scales

Alfonso Senatore, Giuseppe Mendicino, David J. Gochis, Wei Yu, David N. Yates, Harald Kunstmann

Angaben zur Veröffentlichung / Publication details:

Senatore, Alfonso, Giuseppe Mendicino, David J. Gochis, Wei Yu, David N. Yates, and Harald Kunstmann. 2015. "Fully coupled atmosphere-hydrology simulations for the central Mediterranean: Impact of enhanced hydrological parameterization for short and long time scales." *Journal of Advances in Modeling Earth Systems* 7 (4): 1693–1715. https://doi.org/10.1002/2015MS000510.

AGU PUBLICATIONS

Journal of Advances in Modeling Earth Systems

RESEARCH ARTICLE

10.1002/2015MS000510

Key Points:
- Fully coupled model includes lateral surface and subsurface water fluxes
- Lateral redistribution increases soil moisture content compared to control run
- Precipitation and long-term land surface hydrological processes are influenced

Correspondence to:
A. Senatore,
alfonso.senatore@unical.it

Citation:
Senatore, A., G. Mendicino, D. J. Gochis, W. Yu, D. N. Yates, and H. Kunstmann (2015), Fully coupled atmosphere-hydrology simulations for the central Mediterranean: Impact of enhanced hydrological parameterization for short and long time scales, *J. Adv. Model. Earth Syst.*, *7*, 1693–1715, doi:10.1002/2015MS000510.

Received 7 JUL 2015
Accepted 3 OCT 2015
Accepted article online 8 OCT 2015
Published online 2 NOV 2015

Fully coupled atmosphere-hydrology simulations for the central Mediterranean: Impact of enhanced hydrological parameterization for short and long time scales

Alfonso Senatore[1], Giuseppe Mendicino[1], David J. Gochis[2], Wei Yu[2], David N. Yates[2], and Harald Kunstmann[3,4]

[1]Department of Environmental and Chemical Engineering, University of Calabria, Rende (CS), Italy, [2]National Center for Atmospheric Research, Boulder, Colorado, USA, [3]Institute of Meteorology and Climate Research-Atmospheric Environmental Research, Karlsruhe Institute of Technology, Campus Alpin, Garmisch-Partenkirchen, Germany, [4]University of Augsburg, Institute of Geography, Augsburg, Germany

Abstract With the aim of developing a fully coupled atmosphere-hydrology model system, the Weather Research and Forecasting (WRF) model was enhanced by integrating a new set of hydrologic physics parameterizations accounting for lateral water flow occurring at the land surface. The WRF-Hydro modeling system was applied for a 3 year long simulation in the Crati River Basin (Southern Italy), where output from the fully coupled WRF/WRF-Hydro was compared to that provided by original WRF model. Prior to performing coupled land-atmosphere simulations, the stand-alone hydrological model ("uncoupled" WRF-Hydro) was calibrated through an automated procedure and validated using observed meteorological forcing and streamflow data, achieving a Nash-Sutcliffe Efficiency value of 0.80 for 1 year of simulation. Precipitation, runoff, soil moisture, deep drainage, and land surface heat fluxes were compared between WRF-only and WRF/WRF-Hydro simulations and validated additionally with ground-based observations, a FLUXNET site, and MODIS-derived LST. Since the main rain events in the study area are mostly dependent on the interactions between the atmosphere and the surrounding Mediterranean Sea, changes in precipitation between modeling experiments were modest. However, redistribution and reinfiltration of local infiltration excess produced higher soil moisture content, lower overall surface runoff, and higher drainage in the fully coupled model. Higher soil moisture values in WRF/WRF-Hydro slightly influenced precipitation and also increased latent heat fluxes. Overall, the fully coupled model tended to show better performance with respect to observed precipitation while allowing more water to circulate in the modeled regional water cycle thus, ultimately, modifying long-term hydrological processes at the land surface.

1. Introduction

Water, energy, and ecological fluxes and processes at and between the atmosphere, the land surface, and the subsurface are strongly tied together [*Rodriguez-Iturbe*, 2000] through highly complex interactions [*Pan and Mahrt*, 1987; *Bates et al.*, 2008]. Various approaches to representing these processes have been reported where surface and subsurface processes are coupled to land surface schemes [e.g., *Tague and Band*, 2004; *Rigon et al.*, 2006; *Fatichi et al.*, 2012; *Niu et al.*, 2014; *Mendicino et al.*, 2015], with meteorological forcing data specified from either observations, meteorological forecasts, or climate scenarios. In these systems, however, indirect interactions with atmospheric layers higher than the surface layer are not modeled, hence surface-subsurface processes interaction, in particular lateral water and soil moisture redistribution, are not able to produce any feedback on the atmospheric processes simulation. Conversely, most of the current meteorological and climate models describe surface and subsurface hydrological processes in an oversimplified way, often adopting a (vertical) one-dimensional approach that does not consider complex effects on surface water and soil moisture patterns produced by geomorphology and complex terrain in combination with soil and surface hydraulic characteristics.

A growing number of studies have shown that revision of land surface, subsurface, and groundwater hydrology to account for more integrated representation of terrestrial hydrologic dynamics can lead to improved performance of the regional and also large-scale water cycle [*Fan et al.*, 2007; *Maxwell and Kollet*,

2008; *Lowrey and Yang*, 2008; *Balsamo et al*., 2011]. In this integrated water cycle modeling framework, fully coupled modeling of atmospheric and hydrological processes is a topic of growing interest among hydrometeorologists, hydroclimatologists, and traditional hydrologists alike, because the possibility of including soil moisture redistribution feedback in the lower boundary condition of meteorological models, portends an improvement in process representation of water and energy fluxes modeling between land and the atmosphere. Additionally, fully coupled land-atmosphere modeling systems offer significant potential for unified, mass and energy-conserving modeling of the full regional water cycle, from atmospheric processes to river outlets.

The development of novel, fully two-way dynamically coupled atmospheric-hydrological modeling systems has been initiated with the aim of improving hydrometeorological process representation and forecasts and also for providing improved projections of hydrological impacts due to climate and land use changes. First attempts, with short time scale idealized and semiidealized simulations, were performed by *Maxwell et al*. [2007, 2011], which combined the parallel hydrology model ParFlow [*Jones and Woodward*, 2001] first with the Advanced Regional Prediction System (ARPS) [*Xue et al*., 2003], then with the Weather Research and Forecasting atmospheric model (WRF) [*Skamarock et al*., 2008], highlighting that a more detailed representation of lateral surface and subsurface water runoff changes the spatial patterns of land surface fluxes. More recently, *Shrestha et al*. [2014] coupled ParFlow with the COSMO (Consortium for Small-Scale Modeling) [*Baldauf et al*., 2011] atmospheric model and the NCAR CLM (Community Land Model-CLM) [*Oleson et al*., 2008] land surface model (LSM), for 1 week, real-world simulations showing improved predictions of surface fluxes and a strong sensitivity to the initial soil moisture content. *Goodall et al*. [2013] presented a prototype of a modeling system following a service-oriented architecture to connect the Community Atmosphere Model (CAM) [*Neale et al*., 2010], running on a high-performance computer, to the Soil and Water Assessment Tool (SWAT) [*Arnold and Allen*, 1996], running on a personal computer. *Zabel and Mauser* [2013] performed some long-term fully coupled simulations by integrating the MM5 [*Grell et al*., 1994] regional climate model (RCM) (45×45 km^2) and the PROMET [*Mauser and Bach*, 2009] land surface hydrological model (1×1 km^2) over the upper Danube catchment. They found for a 4 year period an improvement for simulated near-surface air temperature and annual average runoff, even though the overall accuracy of the precipitation amounts remained highly uncertain. *Butts et al*. [2014] and *Larsen et al*. [2014] linked the HIRHAM [*Christensen et al*., 1996] regional climate model (11×11 km^2) and the combined MIKE SHE-SWET [*Overgaard et al*., 2007] hydrology and LSM model (500×500 m^2). They performed several 1 year runs on the small Skjern catchment (Denmark), specifically focusing on the data transfer interval between the two models, which run on different operating systems and finding that the coupled model simulations performed more accurately than uncoupled simulations for longer than daily cumulative precipitation. Lastly, *Wagner et al*. [2013] recently coupled WRF and the Hydrologic Model System (HMS) [*Yu et al*., 2006] for a climate and land use changes analysis in the Poyang Lake region (China).

Within the relatively fast growing family of fully coupled atmosphere-hydrology modeling systems, the WRF-Hydro system [*Gochis et al*., 2013] is chosen in this study for assessing effects of fully coupled modeling with respect to the standard column-only land surface modeling approach. Since 2013, WRF-Hydro is freely downloadable as the hydrological extension package of the WRF model (http://www.ral.ucar.edu/projects/wrf_hydro/). WRF-Hydro was originally designed as a model-coupling framework aimed at facilitating easier coupling between WRF and multiple components of terrestrial hydrological models, by accounting for different resolutions between atmospheric and hydrological models through the use of subgrid disaggregation-aggregation procedures. As a first application, this framework was applied for providing the Noah LSM [*Chen and Dudhia*, 2001] with surface overland flow and subsurface saturated flow modules [*Gochis and Chen*, 2003]. More recently, WRF-Hydro has evolved into a more general coupling architecture for coupling hydrological models with atmospheric models while also providing a stand-alone modular fully distributed, multiphysics, multiscale hydrological, and hydraulic modeling system, which is fully parallelized to enable its usage on clusters and high-performance computing systems. Currently, the WRF-Hydro system is being tested and applied in different regions throughout the world, both in uncoupled and fully coupled way [e.g., *Yucel et al*., 2015; *Fersch et al*., 2014] and enhancements are continuously proposed within the WRF-Hydro community (e.g., for integrating the unsaturated and saturated zone to a two-dimensional groundwater scheme). Nonetheless, some versions of the system are already operationally used in various

regions (e.g., Israel Hydrological Service, personal communication, 2015) and tested within several research collaborations, such as the ongoing U.S. National Flood Interoperability Experiment [*Maidment*, 2015].

In this study, WRF-Hydro (version 1.0; described below and in *Gochis et al.* [2013]) is used for assessing impact of fully coupled atmospheric-hydrological modeling on several hydrometeorological variables in a Mediterranean catchment, the Crati River Basin (Southern Italy), for a 3 year simulation period. The main objective of the study is to examine differences induced by the uncoupled and fully coupled approaches for several variables directly connected to land surface modeling, with a particular focus on the impacts of those changes on precipitation. The analysis mainly considers the long-range time scale (e.g., months to seasons) typical for climate modeling, where the final solution is more sensitive to boundary forcing and the model physics, even though additionally specific single events at the time scales typical of NWPs are analyzed.

The main impact expected by the fully coupled WRF/WRF-Hydro modeling of lateral soil surface and subsurface fluxes is an increase of soil moisture content. This effect should occur because:

1. Soil columns located at higher elevations, where usually higher precipitation amounts are observed, are less likely to reach saturation because, depending on the steepness, their water content can be redistributed to downstream neighboring soil columns.
2. Accumulated surface runoff in WRF-Hydro, generated either by infiltration excess or saturation excess mechanisms, can route and reinfiltrate before reaching channel network, avoiding to be removed from the modeled water cycle (in the fully coupled WRF/WRF-Hydro, water eventually reaching the channel—or the aquifer through deep drainage—is only one-way modeled and cannot come back to the soil or the atmosphere).

All else being equal, the combined effects of lateral distribution and reinfiltration should lead, besides an increase in soil moisture, to lower runoff, higher soil drainage rates, and higher latent heat fluxes. All these effects should be evident especially in conditions where the soil is not fully saturated and the steep morphology makes more relevant surface and subsurface water lateral redistribution simulation. In addition, summer days with higher temperatures should highlight the contribution within the land surface heat fluxes simulation.

The procedure followed for comparing fully coupled WRF/WRF-Hydro, WRF-only, and uncoupled WRF-Hydro simulations is made up of several steps that will be explained in detail. In the next section, after a description of the study area, data, and the modeling systems, WRF-Hydro is applied as a stand-alone hydrological model, using spatially distributed forcing data derived from ground-based observations of meteorological variables. The aims of the uncoupled WRF-Hydro simulations are (1) assessing the reliability of the model for the study area and (2) parameter calibration and model validation. Then, in section 3, the comparison of WRF-only and fully coupled WRF/WRF-Hydro simulations will be carried out focusing on precipitation, near-surface and surface temperature, runoff, drainage, soil moisture at different depths, and surface heat fluxes, at both short-range and long-range time scales. Lastly, model simulation performance with respect to streamflow from the fully coupled WRF/WRF-Hydro will be assessed.

2. Data and Methods

2.1. Study Area and Ground-Based Observations

The drainage basin analyzed in this study is the Crati River Basin which discharges at the "Santa Sofia" gauging station, a few kilometers upstream the Tarsia Dam, in the Calabria Region (Southern Italy, Figure 1c). The basin is characterized by some peculiar features. Geologically, the terrain encompassing the basin, respectively, the Sila Plateau to the South and East and the Coastal Chain to the West, are characterized by igneous and continental-derived metamorphic units, which are distinct from the carbonate units typical of the main mountain range of peninsular Italy, the Apennine Mountains. The so-called "Calabrian Arc" of this region of Southern Italy has been interpreted as a fragment of the Alpine Chain that overthrusted the Apennine orogenic belt. The mean altitude of the basin is about 675 m a.s.l., with the maximum located at the Sila Plateau (1856 m a.s.l.), and the minimum at the basin outlet (67 m a.s.l.), and almost 40% of the area above 1000 m. Mountains surround a small but significant floodplain, the Crati Valley, by far the most densely populated region of the basin (more than 250,000 inhabitants).

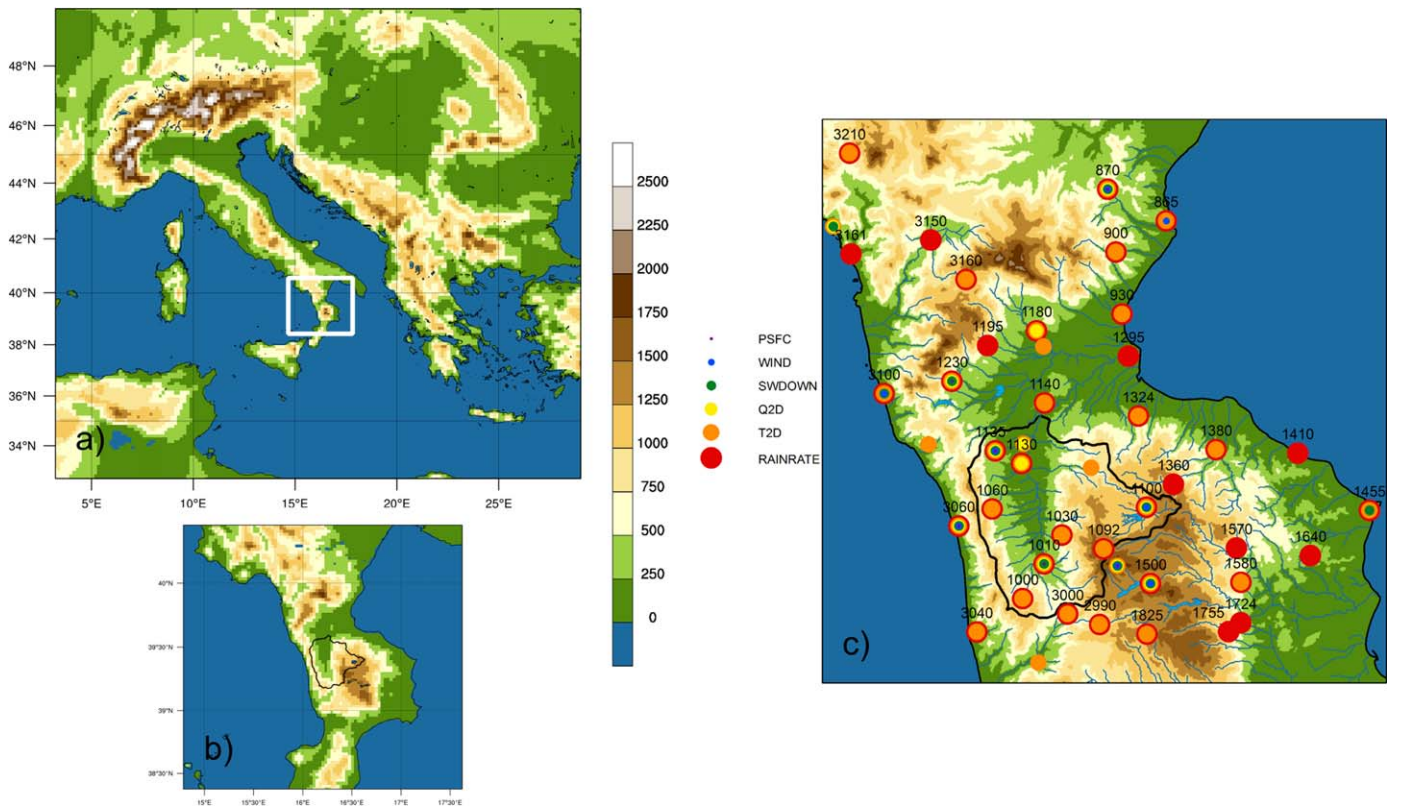

Figure 1. (a) Outer domain, borders of the inner domain are shown (resolution 12.5 km); (b) inner domain; Crati catchment boundaries are also shown (resolution 2.5 km); (c) zoom on the Crati catchment (resolution 250 m), with details about ground-based observation stations used for both off-line model calibration and further performance evaluation. Rain gauge stations IDs are shown.

The climate of the Crati River Basin is also significantly distinct from other large Italian river systems located further north that originate from continental-Apennine zones, whereas almost the entire Crati basin can be considered as within a Mediterranean zone both climatically and biogeographically. The mean annual precipitation in the period 1961–2014 is about 1175 mm, with a decreasing trend of 3.3 mm/yr (level of significance $p = 0.1$ with Mann-Kendall test) and only 18% of the rainfall occurring between May and September. For the same period, mean annual temperature is 12.0°C, varying from 4.2°C in January to almost 21.0°C in July and August, with an increasing trend of 0.13°C/decade ($p = 0.01$; for both precipitation and temperature, monthly series are achieved from the spatial interpolation of data recorded by long-time meteorological stations within and around the basin, and then averaging gridded values for the basin area). *Senatore et al*. [2011] analyzed the hydrological impact of regional climate change projections (2070–2099 versus 1961–1990) in the Crati River Basin with a one-way model-coupling procedure, which predicted mean annual reductions for both root zone soil moisture, groundwater storage, and surface runoff.

The Santa Sofia gauging station is located at the mouth of the 1281 km^2 catchment (with the main river channel length of about 59.1 km) and provides observed river stage and flow rate data since 2001. However, in March 2006, a flood event significantly changed the shape of channel at the outlet and affected the local rating curve. Hence, the selected study period ranges from October 2002 to September 2005 (3 hydrological years), so it is assumed that the rating curve used for deriving discharge data from water levels is reasonably reliable. It is noteworthy that within the basin the Cecita Dam is placed downstream of a small subcatchment of 157 km^2 and also influences the runoff at Santa Sofia gauging station by means of regulation of the dam's outflow volumes mainly for hydroelectric purposes. Ground-based observations of variables used to construct gridded meteorological forcing data for stand-alone WRF-Hydro simulations included, for the analyzed period 2002–2005, 8 pluviometers, 10 thermometers, 3 radiometers, 5 hygrometers, 2 anemometers, and 2 barometers within the catchment boundaries, plus several others around it (Figure 1c).

Table 1. Main WRF Model Physical Options Used for the Study Area

Physics Categories	Selected Option	Reference
Microphysics	Purdue Lin	*Chen and Sun* [2002]
Cumulus parameterization	Mellor-Yamada-Janjic (MYJ)[a]	*Janjic* [2002]
Planetary boundary layer	Kain-Fritsch	*Kain* [2004]
Land surface model	Unified Noah LSM	*Chen and Dudhia* [2001]
Longwave radiation	Rapid Radiative Transfer Model (RRTM)	*Mlawer et al.* [1997]
Shortwave radiation	Dudhia	*Dudhia* [1989]

[a]Only for the large domain.

2.2. The Fully Coupled Modeling System

2.2.1. Advanced Research WRF

The Advanced Research WRF (ARW) model (version 3.5.1) is used for both WRF-only and fully coupled WRF/WRF-Hydro modeling over the study region. Two one-way nested domains are considered: a large domain, with a 12.5 km (172 × 154 grid points) horizontal resolution covering the central region of the Mediterranean basin (32.6°N–49.9°N, 3.1°E–29.1°E; Figure 1a), and a small domain, with a 2.5 km (95 × 90 grid points) horizontal resolution, covering an area (38.4°N–40.5°N, 14.8°E–17.6°E) corresponding mainly to central-northern Calabria (Figure 1b). It is important to note here that in the WRF/WRF-Hydro experiments, WRF-Hydro's routing components are only executed on the innermost domain. This is mainly a computational limitation, however due to the coarse spatial resolution of the outer domain, applying routing components also on it would very unlikely produce significant variations to the results in the inner domain. Time steps are 60 and 12 s, in the large and in the small domain, respectively. The vertical structure of both domains consists of 44 levels, up to a 50 hPa pressure top (about 20 km). Initial and lateral atmospheric boundary conditions for continuous runs are given by the ERA-Interim reanalysis [*Dee et al.*, 2011], but Sea Surface Temperature (SST) fields are directly ingested from the NCEP Real-Time Global SST (NCEP RTG) data set. For SST, also the *sst skin* option is used, which allows to improve the available daily time resolution through the reproduction of the SST diurnal variation from the energy budget over the sea surface, accounting for the cooling effect of longwave radiation and the warming effect of solar insolation [*Zeng and Beljaars*, 2005]. Ancillary data like land cover and soil categories are also replaced by more detailed data sets available for the small domain (specifically, the Corine Land Cover 2006 project for land cover and a detailed soil texture map of Calabria for soil categories) [*ARSSA*, 2003].

The WRF physics parameterization for the selected domains is explained in detail in *Senatore et al.* [2014] and is listed in Table 1. Cumulus parameterization is used only for the coarser grid, while explicit convection is chosen for the finer grid according to *Skamarock et al.* [2008]. The Noah LSM is used as the column land surface physics model in both WRF-only and WRF/WRF-Hydro simulations. The one-dimensional Noah LSM simulates soil moisture (both liquid and frozen), soil temperature, skin temperature, snowpack depth, snowpack water equivalent, canopy water content, and the energy and water flux terms at the earth's surface [*Ek et al.*, 2003]. The column hydrological processes accounted for in the Noah LSM are throughfall, evaporation from both wet canopy and soil, transpiration from dry canopy, soil infiltration, vertical soil water movement along four soil layers, and accumulation of both surface (infiltration excess or ponded water) and underground runoff (free drainage at the bottom of the four soil layers), which are eventually expelled from the overall simulated water cycle. In the soil column configuration used in this study, the depths of the bottom of the layers are, respectively, 0.05, 0.25, 0.70, and 1.50 m. In the fully coupled WRF/WRF-Hydro application, the Noah LSM is enhanced for modeling lateral water distribution and additional relevant hydrological processes as described next.

2.2.2. WRF-Hydro

A complete description of the WRF-Hydro system version 1.0 is available in *Gochis et al.* [2013]. While the WRF-Hydro system contains several options for representing distributed hydrologic processes and for representing channel flow, only those options used in the model experiments presented here are described. The main enhancement of WRF-Hydro is the routing of both infiltration capacity excess and saturated subsurface water. Specifically, routed infiltration capacity excess, together with additional possible exfiltration from fully saturated soil, is now not simply removed from the system, but rather is allowed to pond on the land surface, move laterally and reinfiltrate if suitable conditions are met.

With respect to other coupled modeling systems approaches, hydrological components of the fully coupled modeling system run using the same model executable and the same operating system as the atmospheric components. The hydro model components are fully interactive with the Noah LSM and WRF model physics and are called and interact at every LSM time step of the inner domain (12 s in our case). Model state and flux variables relevant to hydrological component coupling are passed in memory and parallelization is

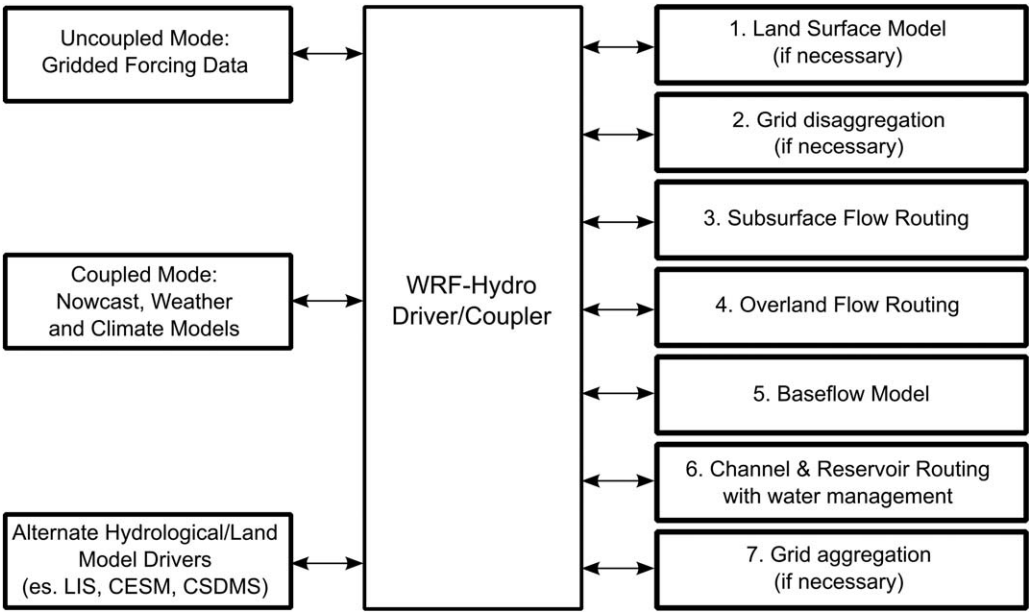

Figure 2. Sketch of the WRF-Hydro modular calling structure [from *Gochis et al*., 2013].

achieved using a similar domain decomposition (or "tiling") approach as is used by the WRF model. The modular calling structure of WRF-Hydro is illustrated in Figure 2, while below some essential details of the modeling system are provided. For further information about technical description and model physics options, the reader is referred to *Gochis et al*. [2013].

2.2.2.1. Fully Coupled Processes: Subsurface and Surface Overland Flow Routing

Since redistribution of terrestrial moisture mainly depends on the dominant local landscape gradient features and because estimation of those gradients is highly scale dependent, WRF-Hydro employs a multiscale modeling approach. The subgrid disaggregation-aggregation procedure is described in *Gochis and Chen* [2003]. Specifically, a disaggregation loop is run after the main LSM loop and prior to routing of saturated subsurface and surface water. In this way, specific hydrologic state variables (namely maximum soil moisture content for each soil type, infiltration excess, lateral saturated conductivity for each soil type, and soil moisture content for each soil layer) are divided up from the LSM grid square into integer portions according to an aggregation factor. In this study, the aggregation factor is equal to 10, i.e., starting from a 2.5 km LSM resolution in the small domain, hydrological routing is performed at 250 m resolution, which proved to be enough detailed to describe the river network up to at least the fifth Strahler order. To preserve the subgrid, the soil moisture spatial variability structure from one model time step to the next, linear subgrid weighting factors are assigned. These values indicate the fraction of the total land surface model grid value that is partitioned to each subgrid pixel.

Subsurface lateral flow is calculated prior to the routing of overland flow to allow exfiltration from fully saturated grid cells to be added to the infiltration excess calculated from the LSM. The method used to calculate the lateral flow of saturated soil moisture is that suggested by *Wigmosta et al*. [1994] and *Wigmosta and Lettenmaier* [1999] within the Distributed Hydrology Soil Vegetation Model (DHSVM). It calculates a quasi-3-D flow, which includes the effects of topography, saturated soil depth, and depth-varying saturated hydraulic conductivity values. WRF-Hydro specifies the water table depth according to the depth of the top of the highest (i.e., nearest to the surface) saturated layer.

Overland flow routing is achieved using a fully unsteady, explicit, finite difference, diffusive wave approach similar to that of *Julien et al*. [1995] and *Ogden* [1997]. The diffusive wave equation accounts for backwater effects and allows for flow on adverse slopes. While the overland flow routine can be applied in either a two-dimensional or steepest descent approach, here we use the steepest descent method. To maintain model stability and prevent numerical dispersion of overland flood waves, a conservative time step of 5 s for the routing grid is chosen in this study, which meets the Courant condition criteria for diffusive wave

routing on a 250 m resolution grid. Following execution of the routing schemes, the fine grid values are aggregated back to the native land surface model grid. Variables that need to be aggregated, so that the updated values are used on the next iteration of the LSM, are the depth of ponded water (accounting for surface routing) and soil moisture content for each soil layer (accounting for subsurface routing).

2.2.2.2. One-Way Processes: Channel and Reservoir Routing, Base Flow Model

Channel flow routing is performed using an explicit, one-dimensional, variable time stepping diffusive wave formulation. A first-order Newton-Raphson solver is used to integrate the diffusive wave flow equations, with an initial value of the time step equal to that of the overland flow routing time step. Overland flow discharging into the stream channel is not explicitly represented by means of subgrids, but through a simple mass balance analysis. Inflow to stream channel occurs when the ponded water depth of specific grid cells, assigned to a predefined stream channel network, exceeds a fixed retention depth. Channel routing is performed on a pixel-by-pixel basis along the channel network grid. The channel network has a trapezoidal geometry; its parameters (side slope, bottom width, and roughness) are "a priori" defined as Strahler stream order functions. Currently no overbank flow is simulated.

The impact of lakes and reservoirs on hydrological response is achieved through a simple mass balance, level-pool lake/reservoir routing module based on the level pool routing method [*Chow et al*., 1988]. Lakes and reservoirs are conceptually differentiated because reservoirs contain both orifice and weir outlets for discharge, while lakes only contain weirs. Fluxes into a lake/reservoir object occur through the channel network and when surface overland flow intersects a lake object. Fluxes from lake/reservoir objects are considered only through the channel network (currently no fluxes from lake/reservoir objects to the atmosphere or the land surface are represented). The level pool scheme tracks water elevation changes over time, while outflows are functions of the water elevation and spillway parameters.

Finally, base flow to the stream network is represented using a simple, empirically based bucket model. This model, especially useful for long-term simulations, is linked to WRF-Hydro through the deep drainage discharge from the land surface soil column. Several groundwater/base flow subbasins can be specified within a watershed (in our case the whole basin is hypothesized). For each of them, WRF-Hydro uses an exponential function to achieve the bucket discharge as a function of a conceptual water depth in the bucket. Estimated base flow discharged from the bucket model is then combined with lateral inflow from overland flow and is input directly into the stream network as "stream inflow". The total basin base flow flux to the stream network is equally distributed among all channel pixels within a basin.

2.2.3. Stand-Alone WRF-Hydro Calibration

Before analyzing the impact of enhanced hydrological parameterization in the WRF modeling system, WRF-Hydro is run in a stand-alone mode forced by observed meteorological forcing data, with the aim of evaluating its reliability for the analyzed hydrological context and of calibrating its most relevant parameters.

Meteorological forcing input includes incoming shortwave and longwave radiation, air humidity, temperature, pressure, wind speed, and precipitation, with a hourly time step. Different techniques are adopted for creating spatially distributed input fields for each variable starting from point observations, as detailed in Table 2. Typical input parameters required for Noah LSM are needed, grouped in three tables of parameters depending on land cover type, on soil type and some general parameters invariant in the domain (e.g., the surface runoff parameter or the coefficient modifying the drainage out the bottom of the last soil layer). Furthermore, four other WRF-Hydro specific tables are needed, with parameters regarding the channel geometry and roughness (both linked to the Strahler stream order), lake location and size, and related weir/orifice parameters, bucket model coefficients and, finally, lateral surface and subsurface water routing parameters (i.e., hydrological and hydraulic parameters like overland roughness or lateral saturated conductivity, linked to either land cover or soil type). Land cover and soil type data sets used on the innermost domain are converted to match the classifications of the default data sets. In addition to the parameters in the tables, two spatially distributed parameters are also tunable, i.e., a scaling factor for overland flow roughness and the surface retention depth.

Due to the high number of variables involved, many traditional calibration methods can require long computational times. Since the primary objective of the study is to show the effects of lateral soil surface and subsurface water fluxes modeling in a mesoscale model, rather than extensively assessing the performance of the hydrological model, the calibration/validation is limited to only the first year of the analyzed period, considering this time interval long enough to evaluate the basic parameter sensitivities.

Table 2. Spatial Interpolation Techniques Adopted for Each of the Meteorological Forcing Variables Required as Input to Uncoupled WRF-Hydro

Meteorological Forcing Variable	Spatial Interpolation Technique
Precipitation	Exponential kriging
Air temperature	Combination of the square of inverse distance interpolation and height-dependent regressions of station data
Air pressure	Combination of the square of inverse distance interpolation and height-dependent regressions of station data
Air humidity	Combination of the square of inverse distance interpolation and temperature-dependent regressions of station data
Wind speed	Merge of observed data with the wind field calculated by Windninja algorithm [*Forthofer*, 2007]
Incoming shortwave radiation	Merge of observed data with the theoretical incoming solar radiation calculated by the "Area Solar Radiation" ArcGIS geoprocessing tool [*Fu and Rich*, 2002]
Incoming longwave radiation	Observed data not available, resampling of data retrieved from Global Land Data Assimilation System (GLDAS), product GLDAS-1, 3 hourly 0.25°, accessible at http://disc.sci.gsfc.nasa.gov/hydrology/data-holdings (last access 18 June 2015)

Calibration is performed with the aim of reproducing the observed hourly hydrograph of the Crati River Basin at the "Santa Sofia" gauging station, and is addressed in two steps: the first step employs a manual calibration with the aim of identifying the most relevant parameters and roughly calibrating them. Specifically, a stepwise approach is adopted, where first the parameters controlling the total water volume and then the parameters controlling hydrograph shape are calibrated. Within the first group, the infiltration scaling factor (REFKDT), surface retention depth (RETDEPRTFAC), and coefficient governing deep drainage (SLOPE) are included. In the second group, surface and channel roughness parameters, saturated soil lateral conductivity (LKSATFAC) or bucket model exponent are considered. With the manual calibration, sensitivity tests on almost all available parameters are performed.

Once the most influential parameters were identified, an automated calibration procedure based on the PEST software [*Doherty*, 2002] is used. This procedure minimizes an objective function, given by the sum of squared deviations between model-generated streamflow and experimental observations, by means of the Gauss-Marquardt-Levenberg method. The parameters involved in the automatic calibration are: the infiltration scaling parameter (REFKDT), Manning roughness coefficients of the channels, the overland flow roughness scaling factor (spatially constant in the domain), the depth of first soil layer bottom, the saturated soil lateral conductivity (LKSATFAC) for sandy loam (the most diffused texture in the basin), the deep drainage coefficient (SLOPE), and the groundwater bucket model exponent.

Results are shown in Figure 3. After a 2 month spin-up time, the calibration period runs from 1 December 2002 at 00:00 UTC to 6 January 2003 at 00:00 UTC (36 days), corresponding to the beginning of the rainy season, while the validation period spans both the second part of the rainy season and the dry season, until 1 October 2003 at 00:00 UTC (268 days). For the calibration period, the validation period and the whole period, Nash-Sutcliffe efficiency coefficient values are equal to 0.93, 0.72, and 0.80, respectively. Despite the high efficiency values, two main shortcomings of the model can be identified: (1) a systematic quick recession, likely due to a weak parameterization of interflow processes. This drawback might also be connected to the oversimplified base flow model. The main flood pulses are dominated by fast surface runoff responses; infiltrated water must first pass slowly through the soil column before contributing to streamflow, well after the event and only as small changes in base flow. Ongoing work seeks to address this issue. (2) The current lake model used in this study is not able to take into account management rules adopted for the Cecita Dam. This is particularly evident in dry seasons, where observed hydrograph values present several small peaks and troughs even though no rainfall occurred.

Overall, the WRF-Hydro hydrological model appears to perform reasonably well for the simulation of the Crati River Basin streamflow, particularly given the strong seasonality of the hydrologic regime. The same set of calibrated parameters is used in the comparison between the WRF-only and the fully coupled WRF/WRF-Hydro simulations.

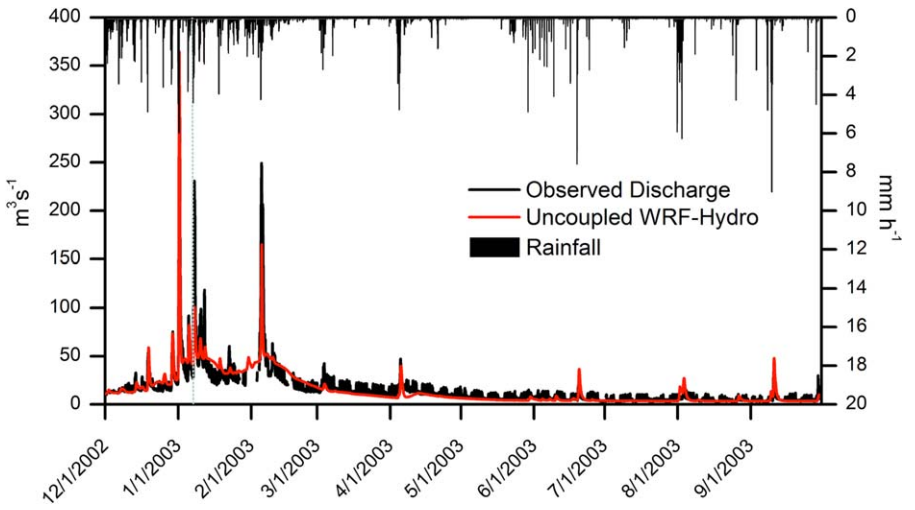

Figure 3. Calibration and validation of the uncoupled WRF-Hydro model for the period 1 December 2002 to 30 September 2003. Gray dotted line in correspondence of 6 January 2003 splits calibration and validation periods.

3. Results and Discussion

The study hypotheses stated in section 1 are all tested in the following, where a comparison between the outputs of both WRF-only and fully coupled WRF/WRF-Hydro models is shown for the analyzed 3 year period. Of course, any comparison between water amounts of various hydrological compartments makes sense only if precipitation inputs are equal or, at least, comparable. This issue is complicated by the fact that soil moisture can significantly influence precipitation [*Findell et al*., 2011]. For this reason, the analysis starts from precipitation.

3.1. Precipitation

Figures 4a and 4b show accumulated multiyear precipitation values in the inner domain during the period November 2002 to September 2005 (October 2002 is run only for spin-up) for both WRF-only and WRF/WRF-Hydro, as well as their differences. The precipitation maps highlight the strong dependence of rainfall patterns on orography. The orographic effect is strongly related to atmosphere interactions with the surrounding sea, and is evident also looking at coarser resolution results (Figure 4d shows outer domain results for the WRF/WRF-Hydro simulation, while Figures 4e and 4f show the convective and nonconvective rain contributions, respectively). The difference map between high-resolution results (Figure 4c) shows some clusters of either overestimation (e.g., in the center or in the north of the domain) or underestimation (e.g., in the south or in the north-east) of WRF-only with respect to WRF/WRF-Hydro, where an unequivocal positive or negative tendency cannot be detected. Considering the whole domain, WRF/WRF-Hydro shows a 2110 mm mean accumulated precipitation value, only 0.4% less than WRF-only (2118 mm); when considering only land cells a 2.3% underestimation is achieved (3422 for WRF/WRF-Hydro versus 3502 mm for WRF-only). If a cell-by-cell comparison is performed for land cells, the WRF/WRF-Hydro absolute percentage differences with respect to WRF-only are higher than 10% only for 12% of the cells.

A comprehensive analysis with respect to ground-based observations from 38 rain gauge stations in the central area of the small domain is shown both in Table 3 and Figure 5. The statistical indices considered are: overall percentage bias, daily Root Mean Square Percentage Error (RMSE) and Stable Equitable Error in Probability Space (SEEPS) [*Rodwell et al*., 2010]. These metrics are calculated on daily basis, which is usually applied for monitoring precipitation forecasts and is selected in this analysis to better account for the prediction of daily dry weather and precipitation amount. Specifically, the 1-SEEPS index is adopted, providing a positively oriented skill score.

With respect to observed values, both WRF-only and WRF/WRF-Hydro show the highest (positive) biases in mountain areas (bias is positively correlated to stations elevation, not shown), while RMSE is generally higher in the eastern side of the region. This outcome is likely caused by the tendency for synoptic frontal systems coming from the West and dropping more rainfall over the interior mountain ranges before

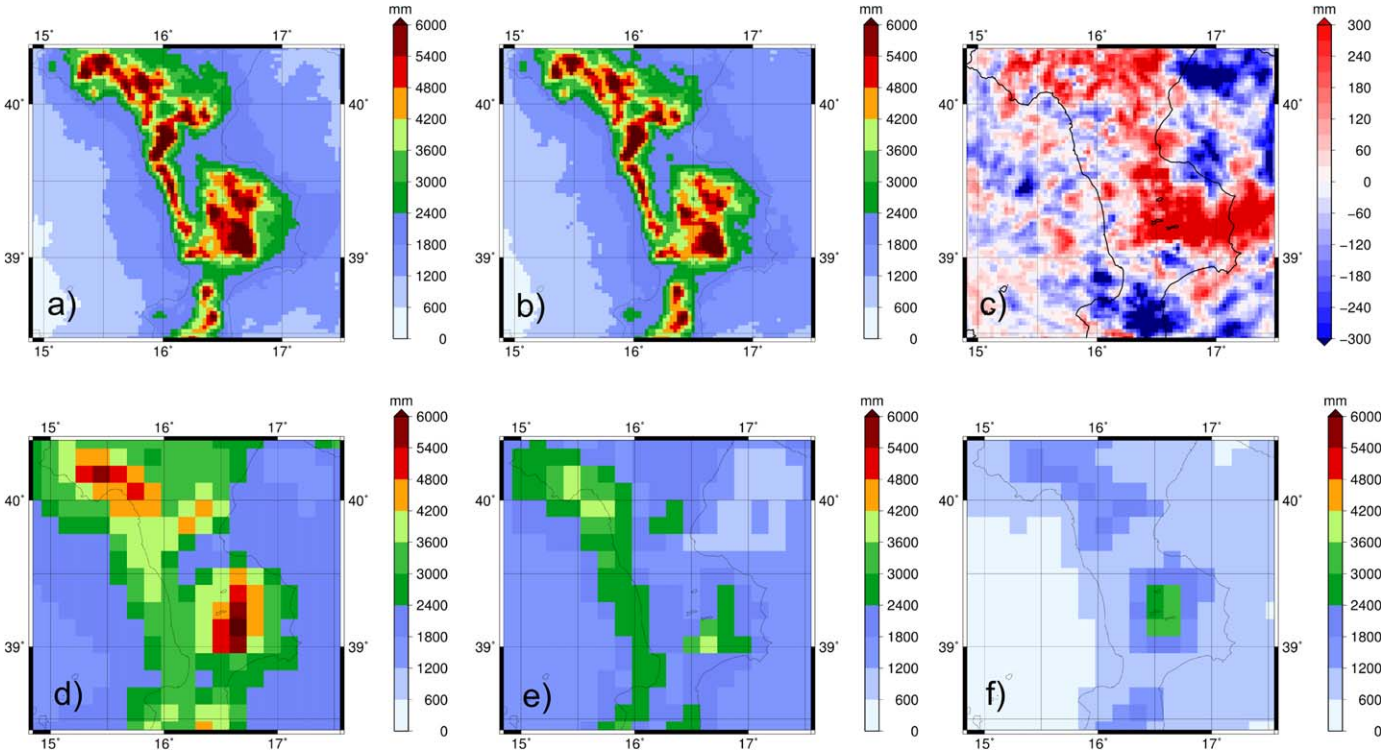

Figure 4. (a) Accumulated precipitation map in the inner domain in the time interval November 2002 to September 2005 with WRF-only simulation; (b) same as Figure 4a, but with fully coupled WRF/WRF-Hydro; (c) difference map (WRF-only minus fully coupled WRF/WRF-Hydro); (d) accumulated precipitation map for the inner domain achieved by outer domain simulation (fully coupled WRF/WRF-Hydro); (e) convective rain contribution in the outer domain simulation; (f) nonconvective rain contribution.

reaching the Eastern coast. 1-SEEPS values are basically constant in the whole area (equal to about 0.5), hence with respect to this index there are no specific zones where either model works significantly better. If WRF-only and WRF/WRF-Hydro performances are directly compared, the largest difference lies in the bias estimates, which are lower with WRF/WRF-Hydro in 66% of cases (25 stations versus 13). Also, the RMSE is generally better with WRF/WRF-Hydro (22 stations versus 16), while with 1-SEEPS WRF-only prevails (22 stations versus 16), even though, as already highlighted, skills are rather similar.

A specific analysis is carried out for the Crati catchment area, where spatially distributed precipitation fields are averaged and compared day by day. Figure 6 shows accumulated mean values for both the whole period and each of the 3 years, together with daily differences of simulated versus observed precipitations. Also in this case, overall accumulated precipitation value is higher with WRF-only (3434 mm), while WRF/WRF-Hydro (3319 mm) is closer to observations (3207 mm). Daily RMSE with respect to observations is equal to 7.3 and 6.4 mm/d, while 1-SEEPS equals 0.58 and 0.60, respectively, for WRF-only and WRF/WRF-Hydro. Absolute differences in daily precipitation values are greater than 10 mm only in 7.3% of cases with WRF and 6.9% of cases with WRF-Hydro. Yearly accumulated precipitation value is not always higher with WRF-only. In the third year, the WRF-only accumulated value is 15 mm lower than WRF/WRF-Hydro (1169 versus 1184 mm), while in the second year the WRF-only overestimation (1284 versus 1187 mm) is mainly due to one single event, occurred on 26 July 2004. The number of days with absolute precipitation differences between the two models higher than 10 mm are very few (only 7 in 1065 days, Table 4), and they usually correspond to an overestimation of observed data. Since the event of 26 July 2004 produces by far the highest precipitation difference between the WRF-only and WRF/WRF-Hydro simulations, it is analyzed in detail next.

The comparison with observations of modeled daily precipitation patterns in the inner domain (Figures 7a and 7b) highlights that both the WRF-only and WRF/WRF-Hydro parameterizations essentially are not able to reproduce the actual rainfall of this specific day. Indeed, some heavy rain was recorded on 26 July 2004 in the south of the domain (less than 60 mm, reasonably reproduced by both the models) and, with a very isolated convective event, in the north of the domain (87 mm, better reproduced by the WRF-only run), but

Table 3. Performance Indices of WRF-Only and Fully Coupled WRF/WRF-Hydro Modeled Precipitation Fields With Respect to Observations From 38 Rain Gauge Stations

Station ID	% Bias WRF	% Bias WRF-Hydro	% RMSE WRF	% RMSE WRF-Hydro	1-SEEPS WRF	1-SEEPS WRF-Hydro
865	27.4	22.3	17.6	17.0	0.486	0.511
870	15.9	17.7	11.6	11.9	0.495	0.493
900	69.7	75.0	19.1	19.7	0.488	0.482
930	9.9	−4.2	15.0	12.1	0.457	0.444
1000	12.5	9.5	8.5	7.5	0.603	0.618
1010	−23.2	−22.6	7.7	7.5	0.514	0.517
1030	1.0	2.3	9.0	8.8	0.484	0.503
1060	17.4	11.1	11.3	9.6	0.495	0.499
1092	53.3	47.7	10.4	9.5	0.497	0.476
1100	16.2	9.3	12.7	10.9	0.518	0.522
1130	−30.1	−28.2	9.7	10.0	0.450	0.442
1135	−30.6	−30.3	8.8	8.7	0.492	0.480
1140	−1.0	−7.1	13.0	13.5	0.488	0.446
1180	11.9	8.6	14.4	14.6	0.469	0.449
1195	20.2	14.4	11.2	12.8	0.520	0.510
1230	18.8	20.9	9.0	9.1	0.563	0.583
1295	12.8	−2.5	14.5	13.9	0.454	0.463
1324	−7.5	−12.0	12.8	13.1	0.474	0.464
1360	10.7	3.8	13.3	10.4	0.491	0.481
1380	−2.3	2.9	12.3	14.7	0.523	0.512
1410	12.3	25.1	15.4	19.3	0.522	0.475
1455	−28.8	−32.4	13.8	14.1	0.444	0.415
1500	25.3	17.7	10.1	9.5	0.461	0.465
1570	97.3	80.7	20.5	16.6	0.420	0.413
1580	58.3	43.5	19.0	16.3	0.461	0.457
1640	25.2	18.2	14.2	12.6	0.515	0.521
1724	45.9	22.0	18.5	13.5	0.514	0.527
1755	52.2	34.4	16.6	13.7	0.526	0.529
1825	32.2	23.6	8.4	7.9	0.546	0.536
2990	−5.2	−11.8	8.3	7.4	0.514	0.513
3000	−11.0	−17.2	8.5	7.1	0.544	0.558
3040	−25.7	−26.0	7.6	8.8	0.469	0.467
3060	15.1	14.8	9.9	8.2	0.509	0.508
3100	−25.9	−22.0	7.6	8.0	0.473	0.473
3150	−26.4	−21.6	6.0	6.4	0.544	0.549
3160	53.1	50.4	11.6	12.1	0.456	0.486
3161	−25.6	−24.3	7.8	8.6	0.536	0.504
3210	−7.5	−11.0	7.1	6.8	0.556	0.565

spatially averaged observed rainfall within the Crati catchment was lower than 5 mm (Table 4). Instead, modeled precipitation passes through the catchment's southern area, with the WRF-only simulation yielding more intense and extended rain. The event is originated by a low-pressure system coming from the Tyrrhenian Sea and crossing region eastward (Figure 8). Upon reaching the Calabrian coast, the WRF-only

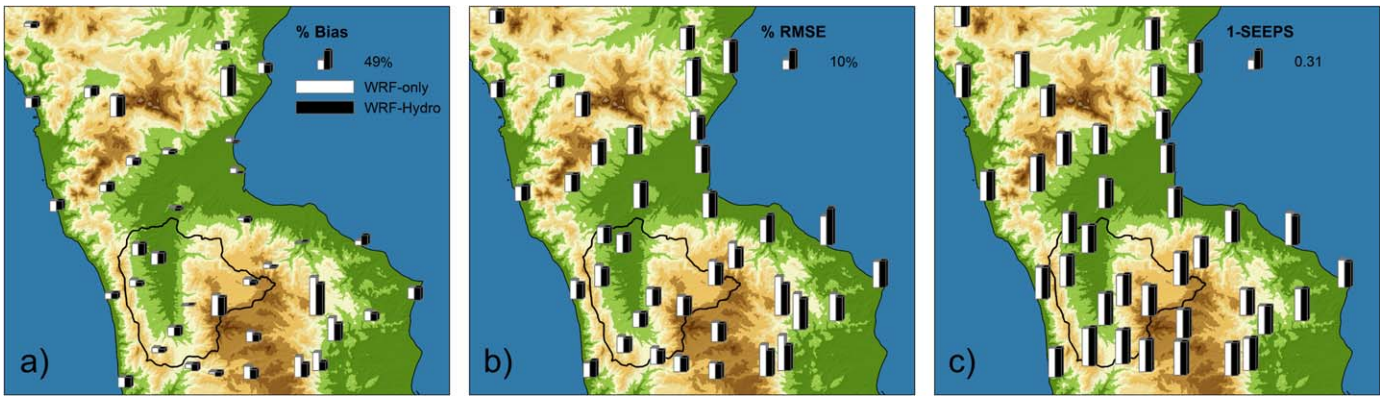

Figure 5. Spatial distribution of the performance indices of WRF-only and fully coupled WRF/WRF-Hydro modeled precipitation fields with respect to observations: (a) percentage bias; (b) Root-Mean-Square Percentage Error; (c) 1-SEEPS.

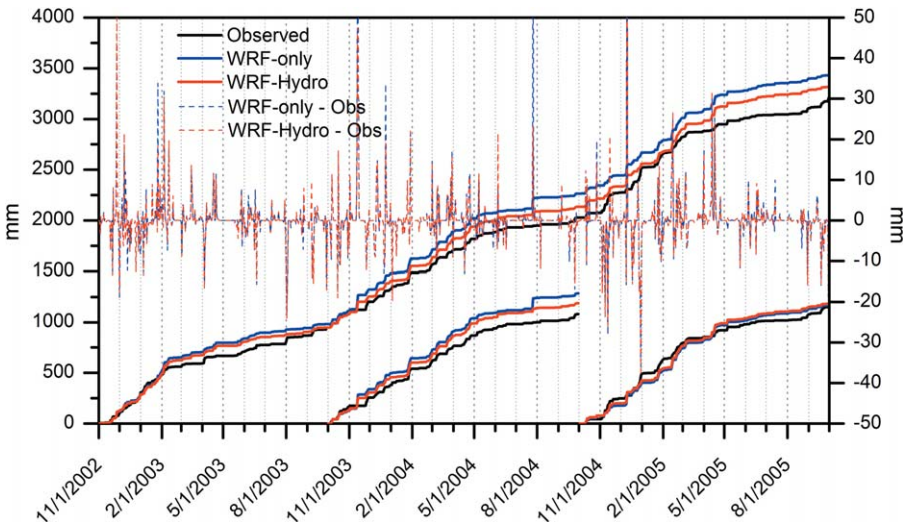

Figure 6. WRF-only, fully coupled WRF/WRF-Hydro and observed accumulated precipitations averaged in the Crati catchment for both the period November 2002 to September 2005 and for yearly subperiods, together with the daily differences of the simulated precipitations with respect to observations.

pressure minimum is already a bit lower than WRF/WRF-Hydro, hence the higher orographic rainfall values along the Tyrrhenian coast should be ascribed to factors not directly dependent on differences between the WRF-only and WRF/WRF-Hydro surface hydrological parameterization. The rain event in the western side of the region is almost finished by 10:00 am UTC, but in the following hours, while the WRF/WRF-Hydro event becomes weaker, the WRF-only modeled rainfall intensity remains high, until it reaches the eastern coast. This behavior is highlighted by the graphs of accumulated rainfall modeled for two rain gauge stations along a West-East axis (Figure 7c). Figure 9 shows a snapshot of column integrated water vapor (IWV), sea level pressure, and 10 m winds at 09:00 am UTC, together with differences in the skin temperature (T_s) for the two models. In the eastern side of the region, not yet affected by precipitation, WRF-only T_s is more than 2 K higher than WRF/WRF-Hydro. A possible explanation of higher rainfall values modeled by the WRF-only in this area can be related to the higher energy provided to the system by warmer surface boundary conditions, that further amplify the WRF-only modeled rainfall event. Since differences in T_s are directly connected to soil moisture values that in turn depend on the way soil moisture distribution is modeled, differences in the modeled precipitation fields in the 26 July 2004 event could be related, at least partially, to differences in the hydrological parameterizations.

Despite the very few cases with significant variations in precipitation simulation, the analyses show that, especially in terms of precipitation volumes, the WRF-only and WRF/WRF-Hydro results are comparable, particularly within the Crati catchment. Hence, the impact of lateral surface and subsurface water distribution operated by WRF-Hydro in the modeling of several hydrological variables can be identified and isolated with reasonable accuracy, as will be shown in the next sections.

Table 4. Days With Absolute Precipitation Differences Between WRF-Only and Fully Coupled WRF/WRF-Hydro Higher Than 10 mm (Average Values in the Crati Catchment)

Day	Observed (mm)	WRF (mm)	WRF-Hydro (mm)	Differences WRF-WRF-Hydro
15 Nov 2004	24.6	29.1	45.5	−16.4
5 Jun 2004	5.9	14.0	27.4	−13.4
24 Dec 2003	4.8	38.5	23.9	14.6
26 Jan 2003	6.5	40.4	24.9	15.5
10 Dec 2002	5.5	17.4	0.5	16.9
14 Nov 2003	0.0	74.5	45.8	28.7
26 Jul 2004	4.8	100.2	27.9	72.3

3.2. Runoff, Drainage, and Soil Moisture

Figure 10 shows accumulated mean values of surface runoff and drainage for the Crati catchment area. As expected, surface and subsurface water lateral redistribution produces a decrease of surface runoff and an increase in percolation from the lowest soil layer. With respect to surface runoff (Figure 10a), WRF-only accumulated values during 3 years almost double that of WRF/WRF-Hydro (1068 versus 641 mm). On

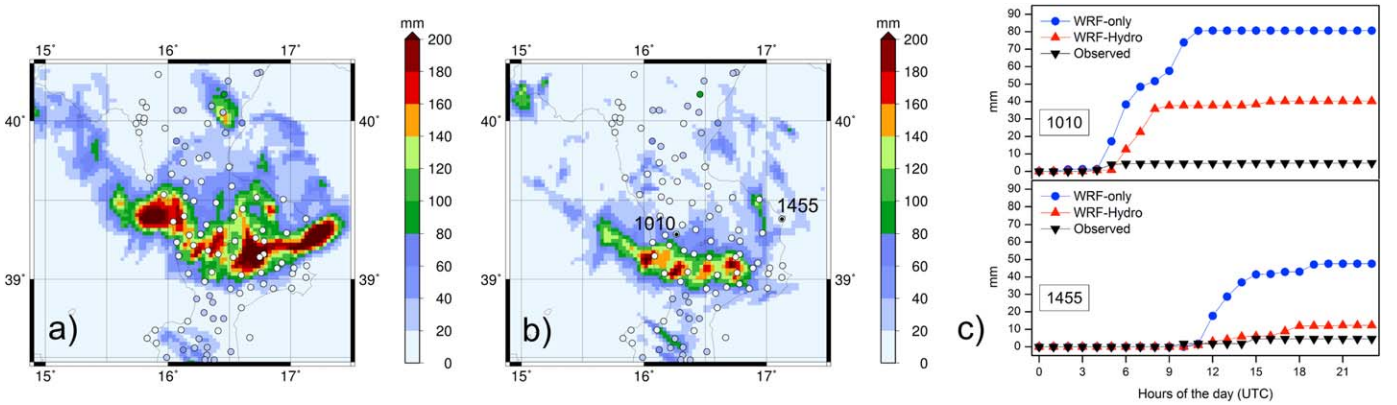

Figure 7. Modeled daily precipitation patterns in the inner domain on 26 July 2004: (a) WRF-only; (b) fully coupled WRF/WRF-Hydro; (c) daily evolution (hourly time step) of observed, WRF-only and fully coupled WRF/WRF-Hydro modeled accumulated precipitation for rain gauge stations 1010 and 1455. Colored circles in Figures 7a and 7b represent observed precipitation values for each recording station available.

average, daily WRF-only values slightly exceed WRF/WRF-Hydro (about 0.4 mm/d), but runoff overestimation occurs almost always (91% of the days with nonzero runoff). A similar but reverse behavior (in this case WRF/WRF-Hydro values are higher than WRF-only) is observed with accumulated drainage (Figure 10b). Accumulated values after 3 years are 893 and 723 mm, respectively, for WRF/WRF-Hydro and WRF-only; day by day drainage excess of WRF/WRF-Hydro with respect to WRF-only is very small (about 0.15 mm on average) but constant (839 days with higher WRF/WRF-Hydro values, 79% of the total). Comparisons between accumulated surface runoff and drainage show that WRF-Hydro enhancements can have significant impacts especially in terms of surface water budget partitioning during long-range simulations and analysis of water resources availability.

Soil moisture differences, while less evident, are responsible for both surface runoff and drainage outcomes. Near-surface (0–0.05 m) soil moisture (Figure 11a) for great part of the first year exhibits practically the same behavior in both models, though some differences in precipitation exist between the two models. At the end of the hot dry season (August–September 2003), when soil moisture content is lower, some higher

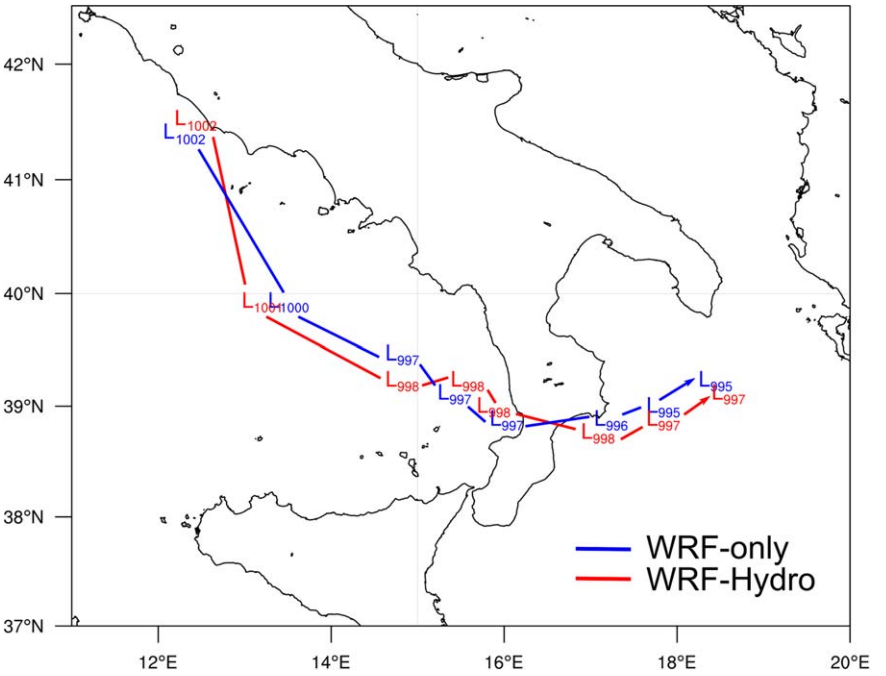

Figure 8. Tracks of pressure minima for both WRF-only and fully coupled WRF/WRF-Hydro simulations calculated from the outer domain. Time steps considered are 15:00 and 21:00 UTC 25 July 2004 and 03:00, 09:00, 12:00, 15:00, 18:00, and 21:00 UTC 26 July 2004.

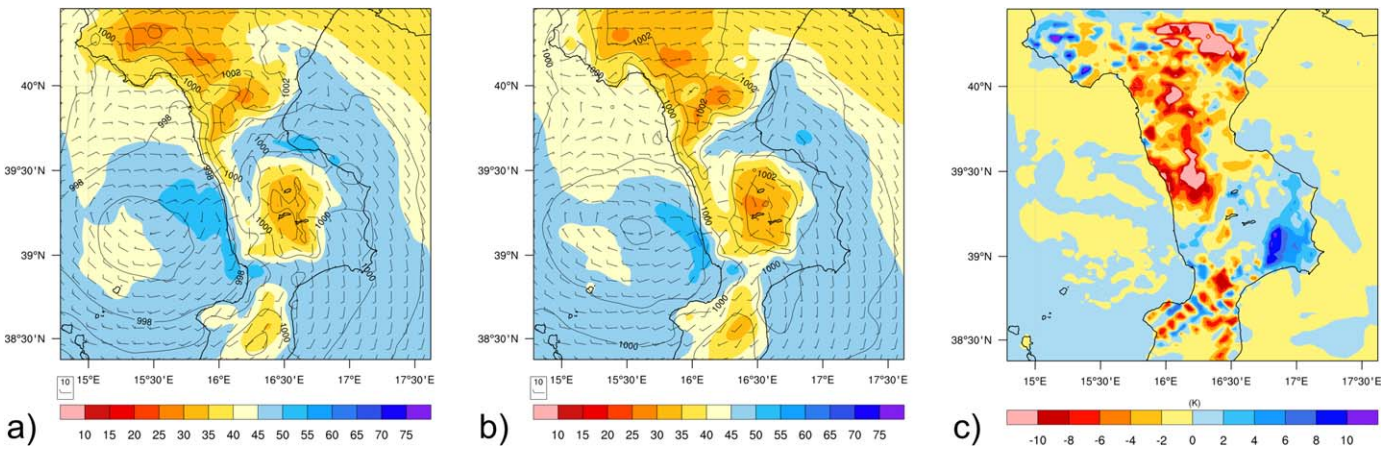

Figure 9. IWV (kg m^{-2}), sea level pressure (contours; hPa), and 10 m winds (barbs; m s^{-1}) on 26 July 2004, 0900 UTC with (a) WRF-only and (b) fully coupled WRF/WRF-Hydro simulations. (c) T_s differences in the skin temperature for the two models (WRF-only minus fully coupled WRF/WRF-Hydro) at the same date and time.

precipitation values with WRF/WRF-Hydro induce a larger increase of average soil moisture that persists until the end of year 2003 even though some stronger WRF modeled rain events occur. During the wet winter, soil moisture evolution again becomes almost identical, because soils tend toward saturation in both cases.

Overall, WRF/WRF-Hydro maintains a longer soil moisture memory with respect to the WRF-only run. The reason for this is explained by the hypotheses expressed in section 1, and is also confirmed by runoff results. Persistence of higher soil moisture values is more evident looking at the fourth (from 0.70 to 1.50 m) soil layer, which is thicker and has a longer response time. Figure 11b shows that every year, especially in autumn and wintertime, WRF/WRF-Hydro soil moisture values significantly exceed WRF-only ones, even with reduced WRF/WRF-Hydro precipitation.

In addition to differences in soil moisture evolution in time, spatial variability of soil moisture fields also show significant differences. Figure 12 highlights first layer soil moisture patterns during a summer day (31 August 2003 at 1:00 P.M. UTC) and a winter day (20 February 2004 at 1:00 P.M. UTC). The first day/hour is chosen because of the relatively high difference between mean soil moisture content in the Crati catchment (0.143 and 0.126, for WRF/WRF-Hydro and WRF-only, respectively), the other instead because for both WRF/WRF-Hydro and WRF-only the same mean soil moisture content (0.265) is modeled. In both cases, a

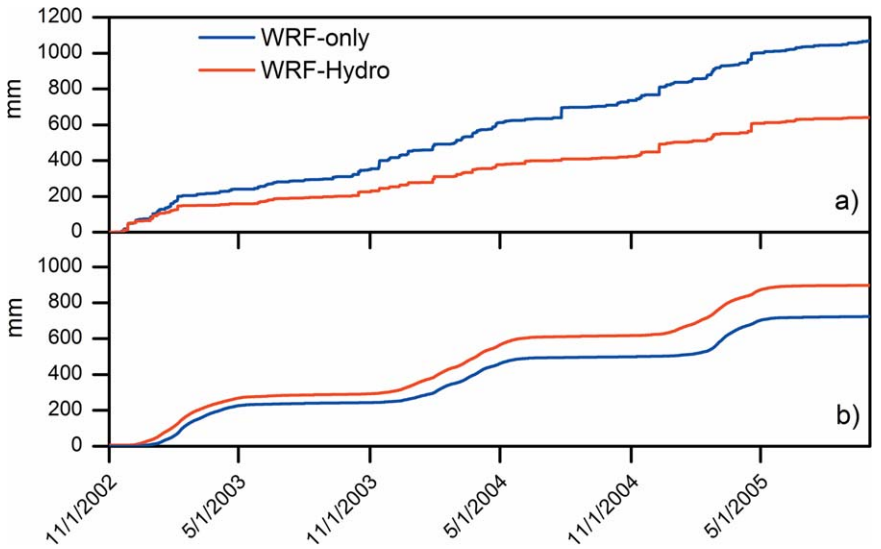

Figure 10. Accumulated values of (a) surface runoff and (b) deep drainage averaged in the Crati catchment area modeled by WRF-only and fully coupled WRF/WRF-Hydro in the period November 2002 to September 2005.

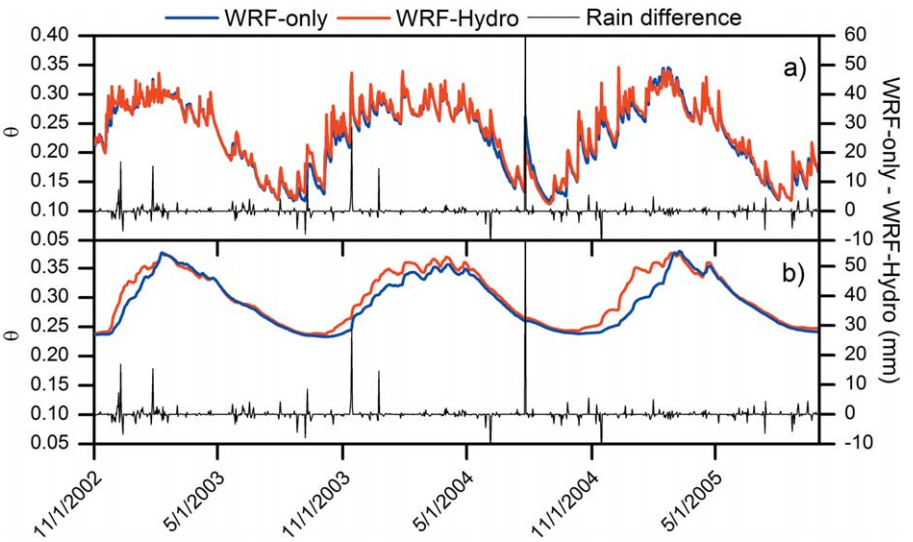

Figure 11. Soil moisture evolution averaged in the Crati catchment area modeled by WRF-only and fully coupled WRF/WRF-Hydro in the period November 2002 to September 2005: (a) first soil layer (from 0 to about 0.05 m below the surface) and (b) fourth soil layer (from 0.70 to 1.50 m).

smoother transition in soil moisture content is observed with WRF/WRF-Hydro moving from wetter mountain slope soils to valley drier soils, especially in the Crati catchment. Smoothness of soil moisture values within the whole inner domain is highlighted also by their frequency distribution (Figures 12c and 12f). In

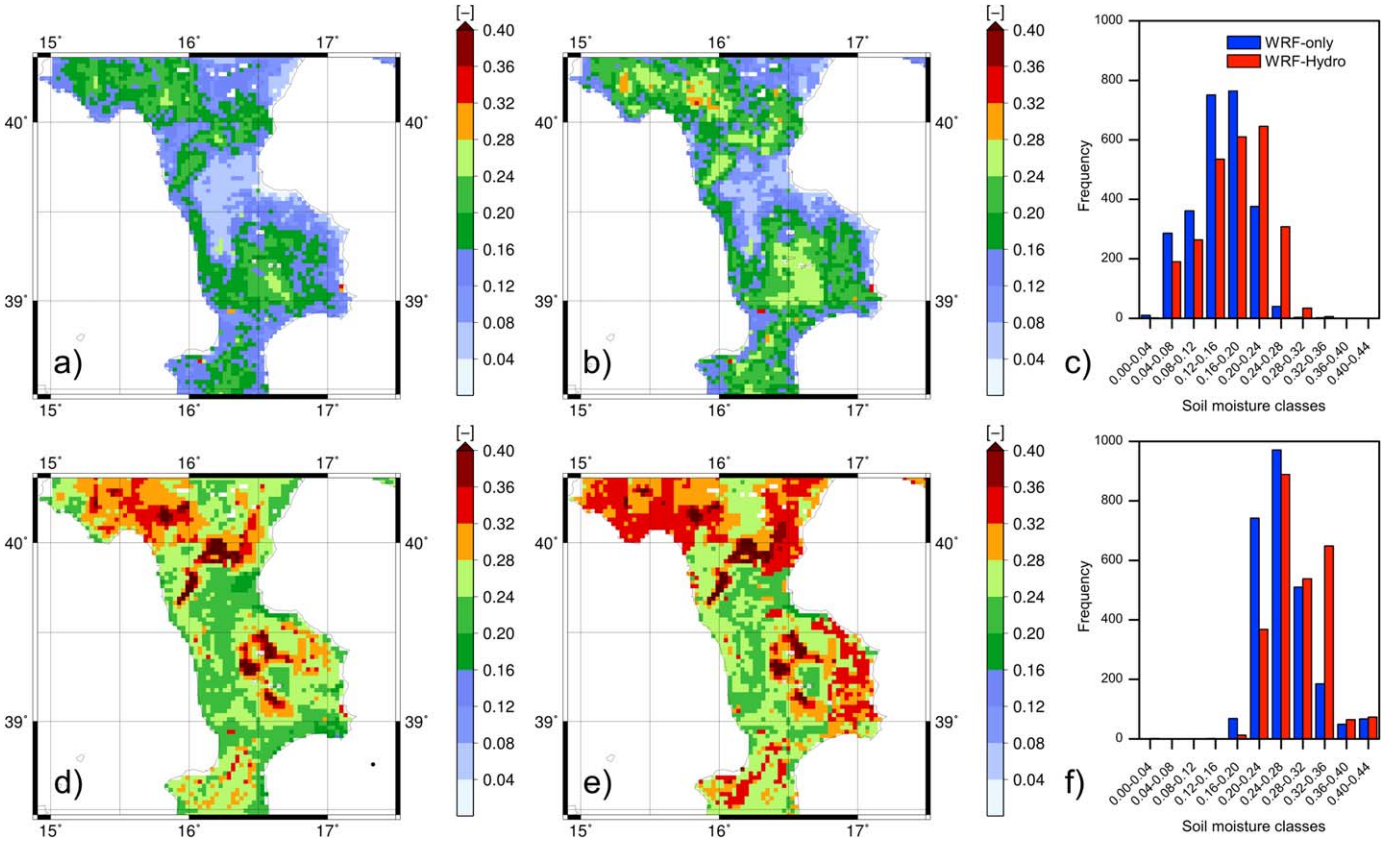

Figure 12. Maps of soil moisture content for the first soil layer: (a) WRF-only, 31 August 2003 at 13:00 UTC; (b) fully coupled WRF/WRF-Hydro, same date and time; (c) comparison of the frequency distribution of soil moisture contents at the same date and time; (d) WRF-only, 20 February 2004 at 13:00 UTC; (e) fully coupled WRF/WRF-Hydro, same date and time; (f) comparison of the frequency distribution of soil moisture contents at the same date and time.

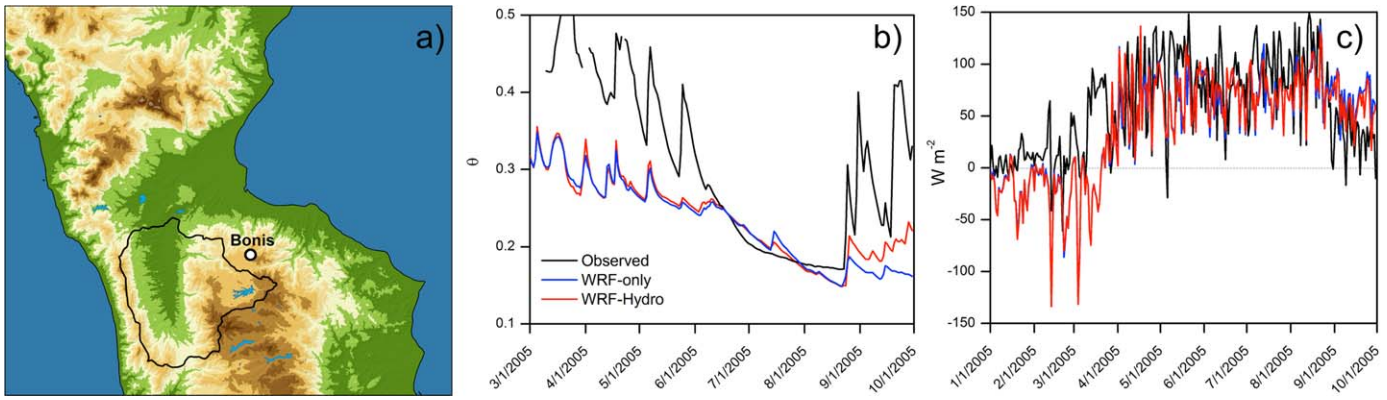

Figure 13. (a) Bonis eddy covariance station location; (b) WRF-only and WRF/WRF-Hydro soil moisture results (0–0.25 cm depth) compared with observations at Bonis site; (c) sensible heat flux H comparison.

both cases, kurtosis is lower with WRF/WRF-Hydro (−0.52 versus −0.30 in summer, 0.84 versus 2.11 in winter). Also the information content provided by the two models can be quantified by means of the information content theory [*Shannon and Weaver*, 1949]. The concept of entropy and information content for estimating the distribution of hydrological variables is widely used [e.g., *Mendicino and Sole*, 1997; *Mendicino*, 1999]. Shannon entropy, meant as a measure of spatial variability, is always higher with WRF/WRF-Hydro (0.77 versus 0.70 and 0.67 versus 0.65, in summer and winter, respectively).

To our knowledge, only one continuous soil moisture measurement is available for models validation in the analyzed area and period, from the Bonis station belonging to the FLUXNET network (http://fluxnet.ornl.gov/site/531, Figure 13a). It is a mountain site (about 1200 m a.s.l.) located in an evergreen needleleaf forest. Soil moisture data are continuously available from March 2005 onward. Figure 13b shows that both models are able to reasonably reproduce observed soil moisture evolution, but inherent uncertainties of the comparison (given, e.g., to the different representative areas of measured and modeled values or to rainfall observations versus estimates) are much higher than differences between models outputs.

More generally, ground-based measurements of variables like soil moisture or surface heat fluxes that can support the validation of fully coupled models are in most cases very seldom available, so they can only partially contribute to models validation (for example, only for few specific combinations of soil and vegetation type). Since remote sensing information is intrinsically spatially distributed, remote sensing techniques can help to overcome this limit [*Hain et al*., 2015]. However, this kind of comparisons adds additional uncertainties related to remote sensing models. An example of a comprehensive spatially distributed validation by means of satellite remote sensing images will be introduced in section 3.3 with surface temperature, a variable whose uncertainty can be managed better than, e.g., surface heat fluxes or soil moisture. Concerning soil moisture patterns, an indirect assessment is performed assuming a relationship between soil moisture and precipitation. Specifically, several weather and climate prediction studies are dealing with duration of soil moisture memory [e.g., *Koster et al*., 2004, 2010]. Our analysis, limited to the Crati catchment area, compares observed and simulated accumulated precipitation, grouped for different classes of first layer soil moisture differences between WRF/WRF-Hydro and WRF-only. Figure 14 shows that for each class, except 0.016–0.020, WRF/WRF-Hydro accumulated precipitation values are closer to observed ones. Despite the overall overestimation of observed precipitation (Figure 6), both WRF-only and WRF/WRF-Hydro overestimate observed precipitation only for differences in soil moisture content lower than 0.008, otherwise (except class 0.016–0.020) they underestimate it. In both cases, however, WRF/WRF-Hydro performs better. In other words, with respect to the WRF-only simulations, if surface and subsurface soil water distribution modeled by WRF/WRF-Hydro leads to a difference in mean soil moisture content negative or positive but lower than 0.008, WRF-Hydro provides a lower overestimate, otherwise it provides a lower underestimate. The differences between WRF-only and WRF/WRF-Hydro precipitation values for each class can be directly linked to surface soil moisture-precipitation interactions. Hence, this result can be assumed as a clear quantification for the analyzed area of the improvement in prediction efficiency given by a more detailed hydrological schematization in the WRF model.

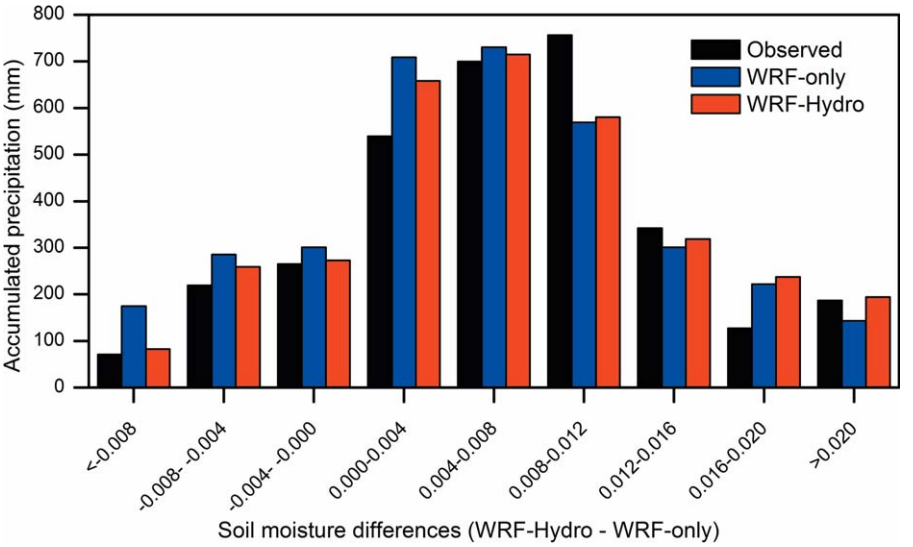

Figure 14. Observed and simulated accumulated precipitations averaged in the Crati catchment, grouped for different classes of first layer soil moisture differences between fully coupled WRF/WRF-Hydro and WRF-only simulations (fully coupled WRF/WRF-Hydro minus WRF-only).

3.3. Air and Land Surface Skin Temperature and Heat Fluxes

Continuous ground-based measurements of 2 m temperature are available for the Crati catchment (Figure 1) that can be considered as a proxy for T_s. Comparisons with observations averaged in the Crati catchment (Table 5) provide similar overall modeled biases (about +0.5 K), which become negative only in wintertime and reach the highest values in summertime. Seasonal differences between WRF-only and WRF/WRF-Hydro modeled temperatures never exceed ±0.1 K, with higher values forecasted by the WRF-only in warm months and lower in cool months. This result is coherent with behavior of drier soils, which heat up more during longer summer daytime (heating is only partially counterbalanced by faster nighttime cooling), but cool down more in winter. Daily biases between WRF-only and WRF/WRF-Hydro values range between −0.8 and +1.5 K. Higher differences are strongly connected to modeled precipitation differences (for example, the highest bias occurs on 14 November 2003, one of the days listed in Table 4).

Table 6 and Figure 15 both show differences between WRF-only and WRF/WRF-Hydro modeled T_s, sensible heat flux (H) and latent heat flux (λE) averaged in the Crati catchment. Specifically, Figure 15a shows that most of the time (73% of the days) WRF-only T_s values are higher than WRF/WRF-Hydro (mean difference is only 0.1 K, 0.2 K in summer). Highest divergences are always linked to differences in modeled precipitation. Variations of modeled T_s are reflected in surface heat flux variables, but the latter are also affected by soil moisture content. Main differences are highlighted roughly during the period May–September. Specifically, in the summer trimester (June–August), WRF-only overestimates H (+6.5 W m^{-2} averagely) and conversely underestimates λE (−7.7 W m^{-2} averagely, −8.7 W m^{-2} in the last year). During summer, λE curves are descending because of lower water availability, while H curves reach their peaks. It is noteworthy that, while in the WRF-only simulations overall mean values of H and λE are almost identical (49.6 and 49.8 W m^{-2}, respectively; Table 6), higher water availability with WRF/WRF-Hydro allows λE to clearly prevail over H (53.6 W m^{-2} versus 46.7 W m^{-2}).

Table 5. Performance Indices of WRF-Only and Fully Coupled WRF/WRF-Hydro Modeled Temperature Fields With Respect to Observations Averaged in the Crati Catchment, for Both the Whole Period December 2002 to August 2005 and Single Seasons (December-January-February, DJF; March-April-May, MAM; June-July-August, JJA; September-October-November, SON)[a]

	December 2002 to August 2005	DJF	MAM	JJA	SON
Observed (K)	286.3	278.5	284.2	295.0	287.6
WRF bias (K)	+0.5 ± 1.2	−0.3 ± 1.0	+0.4 ± 1.0	+0.9 ± 1.3	+1.0 ± 1.4
WRF-Hydro bias (K)	+0.4 ± 1.1	−0.2 ± 1.0	+0.3 ± 1.0	+0.8 ± 1.2	+0.9 ± 1.3

[a]Columns DJF, MAM, and JJA present averaged results from three different time intervals, SON only from two.

Table 6. Differences Between WRF-Only and Fully Coupled WRF/WRF-Hydro Modeled Surface Skin Temperature T_s, Sensible Heat Flux H, and Latent Heat Flux λE Averaged in the Crati Catchment, for Both the Whole Period December 2002 to August 2005 and Single Seasons (DJF, MAM, JJA, and SON)

		December 2002 to August 2005	DJF	MAM	JJA	SON
T_s	WRF (K)	286.5	277.1	284.5	296.6	288.3
	WRF-Hydro (K)	286.4	277.1	284.4	296.4	288.2
H	WRF (W m^{-2})	49.6	−1.0	50.6	102.0	43.6
	WRF-Hydro (W m^{-2})	46.7	−1.2	49.2	95.5	40.0
λE	WRF (W m^{-2})	49.8	22.0	72.9	70.9	24.0
	WRF-Hydro (W m^{-2})	53.6	23.3	74.8	78.6	28.4

As it is shown in the analysis of the 26 July 2004 event (Figure 9), skin temperature differences locally can become significant. Similar to soil moisture content, the λE spatial distribution is analyzed for 31 August 2003 at 1:00 P.M. UTC and 20 February 2004 at 1:00 P.M. UTC (Figure 16). The behavior of the variable is very similar to the soil moisture case, especially for the summer map, with a smoother transition in the WRF/WRF-Hydro run from high λE values (corresponding to wetter soils) to low values (drier soils). Specifically, in both cases, information content is higher with WRF/WRF-Hydro: Shannon entropy equals 0.91 versus 0.83 in summer, but only 0.59 versus 0.58 in winter, when the soil is almost saturated and λE is low.

Direct validation of H with ground-based data is possible from 1 January 2005 in the Bonis site (Figure 13c), but with the same limitations discussed in the case of soil moisture. Spatially distributed T_s validation is performed for 31 August 2003 daily values using the MODIS/Terra V5 LST/E Daily L3 Global 1 km Grid product (MOD11A1), reaggregated at the model resolution (2.5 km). Accuracy of this product is better than 1 K under clear sky conditions [*Coll et al.*, 2009]. Figure 17 shows a comparison of the models and remote sensing map. The main distribution pattern is constrained by terrain elevation, but focusing on some specific areas some significant differences can be observed. In general, MODIS variability is higher and is better represented by WRF/WRF-Hydro, such as shown by a frequency analysis performed over the inland cells of the domain (Figure 17d) and several statistical indices (average value: 307.3, 306.4, and 306.1 K; coefficient of variation: 0.0120, 0.0124, and 0.0144; Shannon entropy: 0.69, 0.72, and 0.77; respectively, for WRF-only,

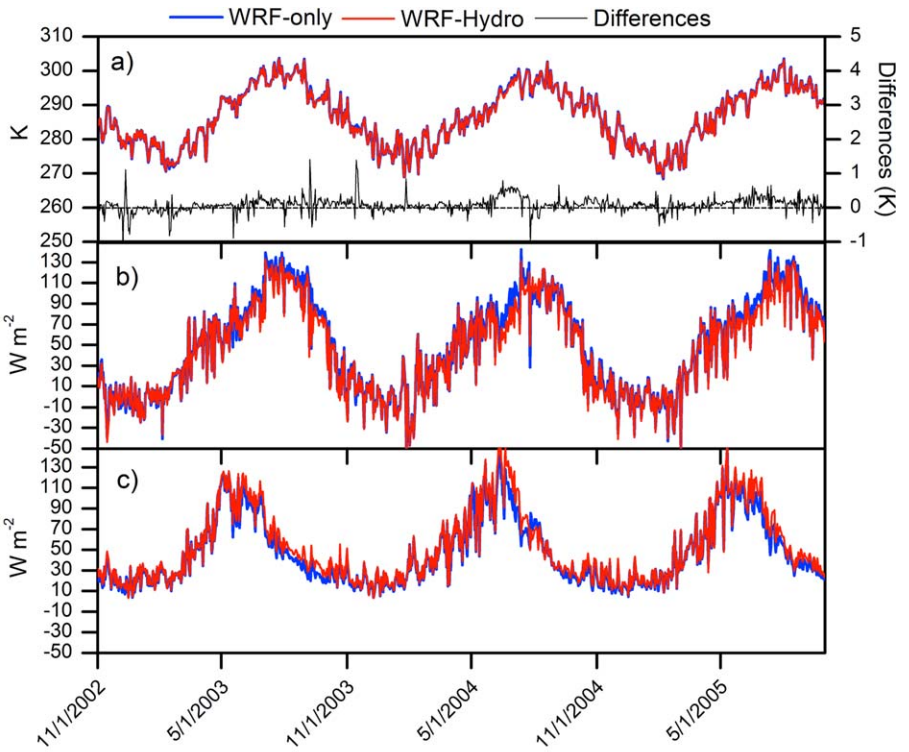

Figure 15. Evolution of several variables averaged in the Crati catchment area modeled by WRF-only and fully coupled WRF/WRF-Hydro in the period November 2002 to September 2005: (a) T_s, the black solid line highlights daily differences (WRF-only minus fully coupled WRF/WRF-Hydro), the black dashed line is the zero line; (b) H; (c) λE.

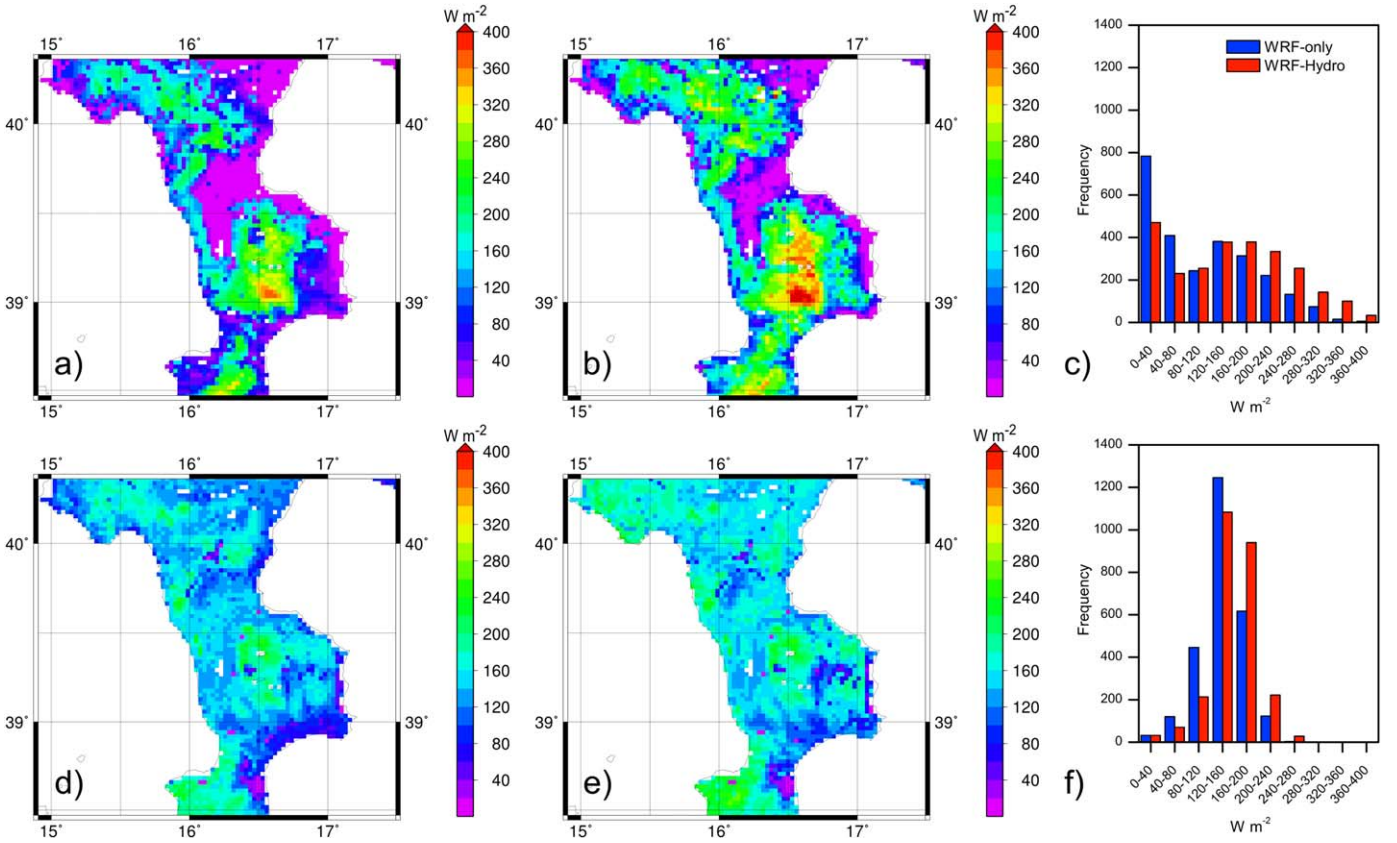

Figure 16. Same as Figure 12, but the analyzed variable is λE.

WRF/WRF-Hydro, and MODIS). In the analysis, coastal cells were skipped because of the clear influence of SST on land cells values. This preliminary spatially distributed validation will be extended and improved in future research.

3.4. Streamflow

Even though channel routing is one-way modeled (i.e., water that has entered the river channel can only flow through the outlet and does not influence other simulated components of the modeled regional water cycle), it is important to assess the performance of the coupled WRF/WRF-Hydro modeled streamflow, since it represents the result of a modeling system that does not require any direct meteorological station observation such as, e.g., precipitation or temperature (at least once a reasonable calibration has been achieved).

Observed and simulated hydrographs for the period from 1 December 2002 to 30 September 2005 at the S. Sofia gauging station are shown in Figure 18. Comparing the 24,872 available observed hourly data (data are missing for less than 3% of the whole period) to simulated hourly runoff in terms of total volumes shows reasonably good results: accumulated observed flow at the outlet reaches 1426×10^6 m^3 at the end of the period, while accumulated simulated flow is 1334×10^6 m^3 (i.e., only 6% less). More important, the ratio with respect to observed/simulated precipitation is equal to 0.36 and 0.34, respectively, for observations and WRF/WRF-Hydro. Nevertheless, the value calculated on 3 years of the Nash-Sutcliffe coefficient is equal only to 0.27, mainly because of the limited reproduction of peak flows, that most of the times are underestimated. Performance degradation with respect to results shown for uncoupled WRF-Hydro calibration is not only related to limited precipitation simulations (both in terms of intensity and duration), but may also be due to the different frequency that the Noah LSM is called in the offline calibration and the fully coupled run.

With version 1.0, when WRF-Hydro is run in offline mode driven by hourly forcing, the land model is typically only called once during that period. In the fully coupled run, instead, the land model (and hence all

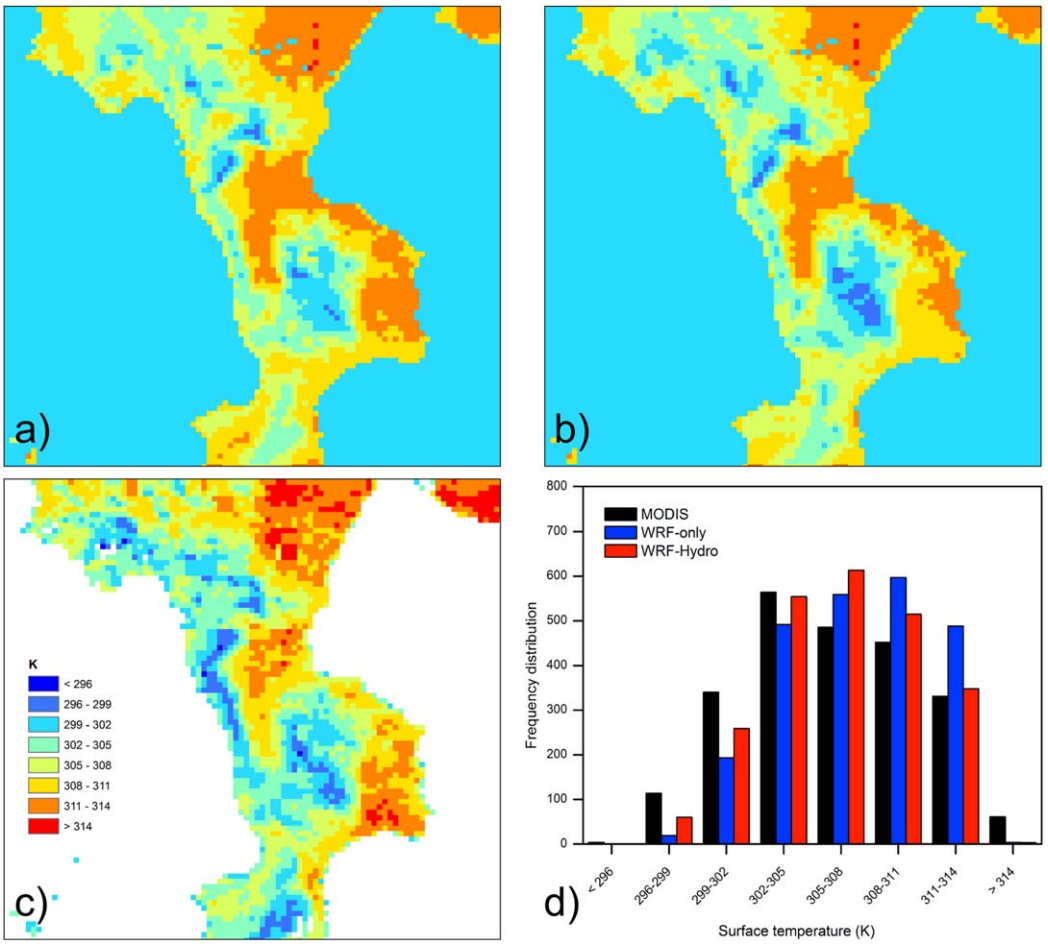

Figure 17. Maps of daily average surface temperature T_s on 31 August 2003: (a) WRF-only, (b) WRF/WRF-Hydro, (c) MODIS MOD11A1 product, and (d) frequency distribution of inland cells T_s values (coastal cells skipped).

the WRF-Hydro routines) is called on the WRF model physics time step, which is in the order of seconds. The difference in land model execution frequency is important because it impacts how frequently infiltration and other fluxes are calculated. If the land model is called infrequently, then routed waters can travel farther downslope or into a channel before infiltration happens again. When the land model is called frequently, infiltration is calculated more frequently and thus more water infiltrates rather than making it all the way into a channel. Hence, more frequent land model calls usually result in more infiltration and less runoff, meaning also lower peak flows. Ongoing work is addressing this latter issue by enabling multiple time steps for the different forcing and model components within WRF-Hydro.

4. Conclusions

A thorough analysis aimed at verifying the impact of enhanced hydrological parameterization in the WRF-ARW model by means of the WRF-Hydro extension package has been carried out in a Mediterranean area, i.e., the Crati catchment, during a 3 year period. Hydrological enhancement mainly consists of explicit representation of lateral surface and subsurface water distribution, with possible reinfiltration of routed surface water, together with additional one-way modeled processes (i.e., channel and reservoir routing, base flow).

The analyzed variables in the comparison study between the stand-alone atmospheric model and the fully coupled atmospheric-hydrological model have been precipitation, near-surface and surface temperatures, surface heat fluxes and runoff, soil moisture, and deep drainage. The largest differences have been shown for surface runoff, where in 3 years WRF-only runs almost doubled WRF/WRF-Hydro values, and in deep

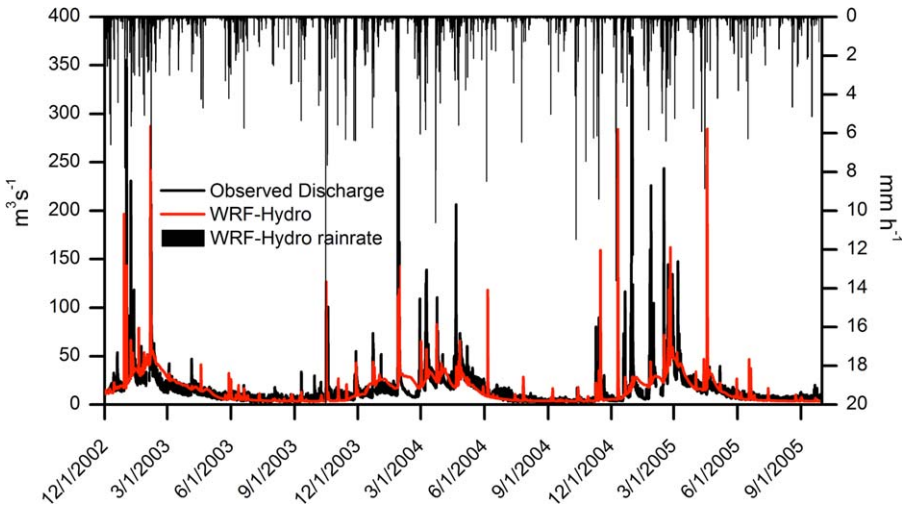

Figure 18. Observed and fully coupled WRF/WRF-Hydro simulated hydrographs for the period 1 December 2002 to 30 September 2005 at the S. Sofia gauging station.

drainage, where conversely WRF/WRF-Hydro values were higher. Also, soil moisture content at various soil layers showed significant variations, especially when drier and warmer atmospheric conditions (summertime) prevented soil saturation. During summertime (that in the analyzed area corresponds to the irrigation season), latent heat flux showed the largest differences, with a greater average estimate of around 8 W m^{-2} for WRF/WRF-Hydro. Soil moisture content and sensible heat flux from both models have been compared with long-term measurements available from a FLUXNET site, while surface temperature with satellite remote sensing estimates, achieving in all cases reasonable results.

Our comparison study has quantified the expected variations in the land surface variables due to the increase of soil moisture content induced by lateral redistribution and reinfiltration allowing water to be removed later from the system via channel flow. Precipitation variation, instead, is more difficult to predict, since its generation in the analyzed area is dominated by sea-atmosphere interactions, rather than land surface soil moisture content alone. Nevertheless, both in the Crati catchment and for 38 available regional rain gauge stations, WRF/WRF-Hydro performances have shown to be slightly better than WRF-only simulations, especially in terms of the bias. Likewise important is that a relationship between differences in soil moisture content and modeled precipitation has been demonstrated for the two models, showing also the positive effect of fully coupled modeling in terms of accumulated precipitation. In terms of WRF-only versus WRF/WRF-Hydro comparison, we expect that the results will broadly remain the same irrespectively of the microphysics scheme used, however it will be interesting in future research to assess the degree of different uncertainties produced by adding the modeling of lateral redistribution of water and using different microphysics schemes.

The issue of improving accuracy in land surface system models is crucial within the ongoing discussion about hyperresolution (0.1–1 km) global hydrology and land surface models [*Bierkens et al.*, 2015; *Singh et al.*, 2015]. The most significant result of this study is probably an answer not only to the question "if," but also "to what extent" does the fully integrated modeling of surface and subsurface water lateral redistribution alter mesoscale model performance in terms of land surface variables and precipitation, at least in the analyzed region. The improvement produced by fully coupled modeling may be even more evident in continental interior regions, where strong convective phenomena are driven by land surface soil moisture, provided that lateral redistribution is significant (no flat areas) and model differences are not blended by all year long near-to-saturation soil moisture conditions (not too humid climate). The results achieved are mainly relevant to long-range simulations, where it is shown that implications especially for the evaluation of water resources availability can be very important. Understanding the impact of the enhanced hydrologic representations on short-term meteorological prediction is somewhat more uncertain and as yet under investigation.

Acknowledgments
The Centro Funzionale Multirischi-ARPACAL (Calabria Region) is acknowledged for providing ground-based observations of meteo-hydrological variables. Giorgio Matteucci from the Italian National Research Council (CNR) is acknowledged for data and further information on the Bonis Fluxnet station. The authors gratefully acknowledge Benjamin Fersch from KIT/IMK-IFU and Thomas Rummler from University of Augsburg for their efforts in the development of the NCAR WRF-Hydro system and for their valuable suggestions. Furthermore, the authors thank Editor Paul Dirmeyer and the anonymous reviewers for their reviews, which helped to improve the quality of this paper. Senatore acknowledges support from the program "Borse Post-doc all'estero UniCal," POR Calabria-European Social Fund 2007/2013, Axis 4 "Capitale umano," Operative objective M.2. D. J. Gochis, W. Yu, and D. N. Yates acknowledge support from the U.S. National Science Foundation under contracts 1234680 and through cooperative agreement support of the National Center for Atmospheric Research (NCAR). The authors acknowledge support by Deutsche Forschungsgemeinschaft and Open Access Publishing Fund of Karlsruhe Institute of Technology. Any information about where to access the data used in this paper, where it is not explicitly mentioned, can be required to the corresponding author, A. Senatore.

References

Arnold, J. G., and P. M. Allen (1996), Estimating hydrologic budgets for three Illinois watersheds, *J. Hydrol.*, *176*(1–4), 57–77.

ARSSA (2003), I suoli della Calabria: Carta dei Suoli in scala 1:250000 della Regione Calabria, Cosenza, Italy.

Baldauf, M., A. Seifert, J. Förstner, D. Majewski, M. Raschendorfer, and T. Reinhardt (2011), Operational convective-scale numerical weather prediction with the COSMO model: Description and sensitivities, *Mon. Weather Rev.*, *139*, 3887–3905, doi:10.1175/MWR-D-10-05013.1.

Balsamo, G., F. Pappenberger, E. Dutra, P. Viterbo, and B. van den Hurk (2011), A revised land hydrology in the ECMWF model: A step towards daily water flux prediction in a fully-closed water cycle, *Hydrol. Processes*, *25*, 1046–1054, doi:10.1002/hyp.7808.

Bates, B. C., Z. W. Kundzewicz, S. Wu, and J. P. Palutikof (Eds.) (2008), Climate change and water, in *Technical Paper of the Intergovernmental Panel on Climate Change*, 210 pp., IPCC Secr., Geneva, Switzerland.

Bierkens, M. F. P., et al. (2015), Hyper-resolution global hydro-logical modelling: What is next?, *Hydrol. Processes*, *29*, 310–320, doi:10.1002/hyp.10391.

Butts, M., M. Drews, M. A. D. Larsen, S. Lerer, S. H. Rasmussen, J. Gross, J. Overgaard, J. C. Refsgaard, O. B. Christensen, and J. H. Christensen (2014), Embedding complex hydrology in the regional climate system—Dynamic coupling across different modelling domains, *Adv. Water Resour.*, *74*, 166–184, doi:10.1016/j.advwatres.2014.09.004.

Chen, F., and J. Dudhia (2001), Coupling an advanced land surface hydrology model with the Penn State-NCAR MM5 modeling system. Part I: Model implementation and sensitivity, *Mon. Weather Rev.*, *129*, 569–585.

Chen, S. H., and W. Y. Sun (2002), A one-dimensional time dependent cloud model, *J. Meteorol. Soc. Jpn.*, *80*, 99–118.

Chow, V. T., D. R. Maidment, and L. W. Mays (1988), *Applied Hydrology*, McGraw-Hill, N. Y.

Christensen, J. H., O. B. Christensen, P. Lopez, E. van Meijgaard, and M. Botzet (1996), The HIRHAM4 regional atmospheric climate model, *DMI Sci. Rep. 96-4*, Dan. Meteorol. Inst., Copenhagen, Denmark.

Coll, C., Z. Wan, and J. M. Galve (2009), Temperature-based and radiance-based validations of the V5 MODIS land surface temperature product, *J. Geophys. Res.*, *114*, D20102, doi:10.1029/2009JD012038.

Dee, D. P., et al. (2011), The ERA-Interim reanalysis: Configuration and performance of the data assimilation system, *Q. J. R. Meteorol. Soc.*, *137*, 553–597.

Doherty, J. (2002), *PEST: Model Independent Parameter Estimation, User Manual*, 4th ed., Watermark Numer. Comput., Brisbane, Queensland, Australia.

Dudhia, J. (1989), Numerical study of convection observed during the winter monsoon experiment using a mesoscale two-dimensional model, *J. Atmos. Sci.*, *46*, 3077–3107.

Ek, M. B., K. E. Mitchell, Y. Lin, E. Rogers, P. Grunmann, V. Koren, G. Gayno, and J. D. Tarpley (2003), Implementation of Noah land surface model advances in the National Centers for Environmental Prediction operational mesoscale Eta model, *J. Geophys. Res.*, *108*(D22), 8851, doi:10.1029/2002JD003296.

Fan, Y., G. Miguez-Macho, C. P. Weaver, R. Walko, and A. Robock (2007), Incorporating water table dynamics in climate modeling: 1. Water table observations and equilibrium water table simulations, *J. Geophys. Res.*, *112*, D10125, doi:10.1029/2006JD008111.

Fatichi, S., V. Y. Ivanov, and E. Caporali (2012), A mechanistic ecohydrological model to investigate complex interactions in cold and warm water-controlled environments: 1. Theoretical framework and plot-scale analysis, *J. Adv. Model. Earth Syst.*, *4*, M05002, doi:10.1029/2011MS000086.

Fersch, B., D. J. Gochis, H. Kunstmann, G. Mendicino, and A. Senatore (Eds.) (2014), *Book of Abstracts of the 1st European Fully Coupled Atmospheric-Hydrological Modeling and WRF-Hydro Users Workshop*, Univ. of Calabria, Rende (CS), Italy. [Available at http://cesmma.unical.it/wrf-hydro2014/BookOfAbstracts.pdf.]

Forthofer, J. M. (2007), Modeling wind in complex terrain for use in fire spread prediction [528 KB], Master thesis, 123 pp., Colorado State Univ., Fort Collins, Colo. [Available at http://www.firelab.org/document/forthofer-thesis.]

Findell, K. L., P. Gentine, B. R. Lintner, and C. Kerr (2011), Probability of afternoon precipitation in eastern United States and Mexico enhanced by high evaporation, *Nature*, *4*, 434–439, doi:10.1038/ngeo1174.

Fu, P., and P. M. Rich (2002), A geometric solar radiation model with applications in agriculture and forestry, *Comput. Electron. Agric.*, *37*, 25–35.

Gochis, D. J., and F. Chen (2003), Hydrological enhancements to the community Noah land surface model: Technical description, *NCAR Sci. Tech. Note TN-454+STR*, 68 pp., National Center for Atmospheric Research (NCAR), Boulder, Colo. [Available at http://nldr.library.ucar.edu/repository/assets/technotes/TECH-NOTE-000-000-000-516.pdf.]

Gochis, D. J., W. Yu, and D. N. Yates (2013), *The WRF-Hydro Model Technical Description and User's Guide, Version 1.0*, *NCAR Technical Document*, 120 pp., NCAR, Boulder, Colo. [Available at http://www.ral.ucar.edu/projects/wrf_hydro/.]

Goodall, J. L., K. D. Saint, M. B. Ercan, L. J. Briley, S. Murphy, H. You, C. De Luca, and R. B. Rood (2013), Coupling climate and hydrological models: Interoperability through web services, *Environ. Modell. Software*, *46*, 250–259, doi:10.1016/j.envsoft.2013.03.019.

Grell, G. A., J. Dudhia, and D. R. Stauffer (1994), A description of the fifth-generation Penn State/NCAR mesoscale model (MM5), *NCAR Tech. Note NCAR/TN-398+STR*, 138 pp., NCAR, Boulder, Colo. [Available at http://nldr.library.ucar.edu/repository/assets/technotes/TECH-NOTE-000-000-000-214.pdf.]

Hain, C. R., W. T. Crow, M. C. Anderson, and M. T. Yilmaz (2015), Diagnosing neglected soil moisture source-sink processes via a thermal infrared-based two-source energy balance model, *J. Hydrometeorol.*, *16*, 1070–1086.

Janjic, Z. I. (2002), Nonsingular Implementation of the Mellor Yamada Level 2.5 Scheme in the NCEP Meso model, *NCEP Off. Note 437*, 61 pp., NOAA/National Weather Service, National Centers for Environmental Prediction (NCEP), College Park, Md. [Available at http://www.emc.ncep.noaa.gov/officenotes/newernotes/on437.pdf.]

Jones, J. E., and C. S. Woodward (2001), Integrated surface-groundwater flow modeling: A free-surface overland flow boundary condition in a parallel groundwater flow model, *Adv. Water Resour.*, *24*, 763–774.

Julien, P., B. Saghafian, and F. Ogden (1995), Raster-based hydrological modeling of spatially-varied surface runoff, *Water Resour. Bull.*, *31*(3), 523–536.

Kain, J. S. (2004), The Kain-Fritsch convective parameterization: An update, *J. Appl. Meteorol.*, *43*, 170–181.

Koster, R. D., et al. (2004), Regions of strong coupling between soil moisture and precipitation, *Science*, *305*, 1138–1140.

Koster, R. D., et al. (2010), Contribution of land surface initialization to subseasonal forecast skill, *Geophys. Res. Lett.*, *37*, L02402, doi:10.1029/2009GL041677.

Larsen, M. A. D., J. C. Refsgaard, M. Drews, M. B. Butts, K. H. Jensen, J. H. Christensen, and O. B. Christensen (2014), Results from a full coupling of the HIRHAM regional climate model and the MIKE SHE hydrological model for a Danish catchment, *Hydrol. Earth Syst. Sci.*, *18*, 4733–4749, doi:10.5194/hess-18-4733-2014.

Lowrey, M. R. K., and Z.-L. Yang (2008), Assessing the capability of a regional-scale weather model to simulate extreme precipitation patterns and flooding in central Texas, *Weather Forecasting*, *23*, 1106–1126.
Maidment, D. R. (2015), A conceptual framework of the National Flood Interoperability Experiment, *NFIE Conceptual Framework Pap.*, 22 pp., Consortium of Universities for the Advancement of Hydrologic Science, Inc. (CUAHSI), Medford, Mass. [Available at https://www.cuahsi.org/Files/Pages/documents/13623/nfieconceptualframework_revised_feb_9.pdf.]
Mauser, W., and H. Bach (2009), PROMET—Large scale distributed hydrological modelling to study the impact of climate change on the water flows of mountain watersheds, *J. Hydrol.*, *376*, 362–377, doi:10.1016/j.jhydrol.2009.07.046.
Maxwell, R. M., and S. J. Kollet (2008), Interdependence of groundwater dynamics and land-energy feedbacks under climate change, *Nat. Geosci.*, *1*(10), 665–669.
Maxwell, R. M., F. K. Chow, and S. J. Kollet (2007), The groundwater-land-surface-atmosphere connection: Soil moisture effects on the atmospheric boundary layer in fully-coupled simulations, *Adv. Water Resour.*, *30*, 2447–2466.
Maxwell, R. M., J. K. Lundquist, J. D. Mirocha, S. G. Smith, C. S. Woodward, and A. F. B. Tompson (2011), Development of a coupled groundwater-atmosphere model, *Mon. Weather Rev.*, *39*, 96–116, doi:10.1175/2010MWR3392.1.
Mendicino, G. (1999), Sensitivity analysis on GIS procedures for the estimate of soil erosion risk, *Nat. Hazards*, *20*, 231–253.
Mendicino, G., and A. Sole (1997), The information content theory for the estimation of the topographic index distribution used in TOPMODEL, *Hydrol. Processes*, *11*, 1099–1114.
Mendicino, G., J. Pedace, and A. Senatore (2015), Stability of an overland flow scheme in the framework of a fully coupled eco-hydrological model based on the Macroscopic Cellular Automata approach, *Commun. Nonlinear Sci. Numer. Simul.*, *21*(1–3), 128–146, doi:10.1016/j.cnsns.2014.08.021.
Mlawer, E. J., S. J. Taubman, P. D. Brown, M. J. Iacono, and S. A. Clough (1997), Radiative transfer for inhomogeneous atmosphere: RRTM, a validated correlated-k model for the longwave, *J. Geophys. Res.*, *102*, 16,663–16,682.
Neale, R. B., A. Gettelman, S. Park, C. Chen, P. H. Lauritzen, and D. L. Williamson (2010), Description of the NCAR Community Atmospheric Model (CAM 5.0), *NCAR Tech. Note TN-486*, Natl. Cent. for Atmos. Res., Boulder, Colo. [Available at http://www.cesm.ucar.edu/models/cesm1.0/cam/.]
Niu, G.-Y., C. Paniconi, P. A. Troch, R. L. Scott, M. Durcik, X. Zeng, T. Huxman, and D. C. Goodrich (2014), An integrated modelling framework of catchment-scale ecohydrological processes: 1. Model description and tests over an energy-limited watershed, *Ecohydrology*, *7*, 427–439, doi:10.1002/eco.1362.
Ogden, F. L. (1997), *CASC2D Reference Manual*, Univ. of Conn., Storrs.
Oleson, K. W., et al. (2008), Improvements to the Community Land Model and their impact on the hydrological cycle, *J. Geophys. Res.*, *113*, G01021, doi:10.1029/2007JG000563.
Overgaard, J., M. B. Butts, and D. Rosbjerg (2007), Improved scenario prediction by using coupled hydrological and atmospheric models, in *Quantification and Reduction of Predictive Uncertainty for Sustainable Water Resources Management*, vol. 313, edited by E. Boegh et al., pp. 242–248, IAHS Press, Wallingford, U. K.
Pan, H.-L., and L. Mahrt (1987), Interaction between soil hydrology and boundary-layer development, *Boundary Layer Meteorol.*, *38*, 185–202.
Rigon, R., G. Bertoldi, and T. M. Over (2006), GEOtop: A distributed hydrological model with coupled water and energy budgets, *J. Hydrometeorol.*, *7*(3), 371–388.
Rodriguez-Iturbe, I. (2000), Ecohydrology: A hydrologic perspective of climate-soil-vegetation dynamics, *Water. Resour. Res.*, *36*, 3–9.
Rodwell, M. J., D. S. Richardson, T. D. Hewson, and T. Haiden (2010), A new equitable score suitable for verifying precipitation in numerical weather prediction, *Q. J. R. Meteorol. Soc.*, *136*, 1344–1363.
Senatore, A., G. Mendicino, G. Smiatek, and H. Kunstmann (2011), Regional climate change projections and hydrological impact analysis for a Mediterranean basin in southern Italy, *J. Hydrol.*, *399*(1–2), 70–92, doi:10.1016/j.jhydrol.2010.12.035.
Senatore, A., G. Mendicino, H.-R. Knoche, and H. Kunstmann (2014), Sensitivity of modeled precipitation to sea surface temperature in regions with complex topography and coastlines: A case study for the Mediterranean, *J. Hydrometeorol.*, *15*(6), 2370–2396, doi:10.1175/JHM-D-13-089.1.
Shannon, C. E., and W. Weaver (1949), *The Mathematical Theory of Communication*, 117 pp., Univ. of Ill. Press, Urbana.
Shrestha, P., M. Sulis, M. Masbou, S. Kollet, and C. Simmer (2014), A scale-consistent terrestrial systems modeling platform based on COSMO, CLM, and ParFlow, *Mon. Weather Rev.*, *142*, 3466–3483, doi:10.1175/MWR-D-14-00029.1.
Singh, R. S., J. T. Reager, N. L. Miller, and J. S. Famiglietti (2015), Toward hyper-resolution land-surface modeling: The effects of fine-scale topography and soil texture on CLM4.0 simulations over the Southwestern U.S., *Water Resour. Res.*, *51*, 2648–2667, doi:10.1002/2014WR015686.
Skamarock, W. C., J. B. Klemp, J. Dudhia, O. D. Gill, D. M. Barker, M. G. Duda, X. Huang, W. Wang, and J. G. Powers (2008), A description of the Advanced Research WRF version 3, *NCAR Tech. Note NCAR/TN-4751STR*, Natl. Cent. for Atmos. Res., Boulder, Colo.
Tague, C. L., and L. E. Band (2004), RHESSys: Regional Hydro-Ecologic Simulation System: An object-oriented approach to spatially distributed modeling of carbon, water, and nutrient cycling, *Earth Interact.*, *8*(19), 1–42.
Wagner, S., B. Fersch, H. Kunstmann, F. Yuan, C. Yang, and Z. Yu (2013), Hydrometeorological modeling for Poyang Lake region, China, in *Proceedings of H01, IAHS-IAPSO-IASPEI Assembly*, *IAHS Publ.*, 359, 152–157.
Wigmosta, M., and D. P. Lettenmaier (1999), A comparison of simplified methods for routing topographically driven subsurface flow, *Water Resour. Res.*, *35*, 255–264.
Wigmosta, M., L. W. Vail, and D. P. Lettenmaier (1994), A distributed hydrology-vegetation model for complex terrain, *Water Resour. Res.*, *30*, 1665–1679.
Xue, M., D. Wang, J. Gao, K. Brewster, and K. K. Droegemeier (2003), The Advanced Regional Prediction System (ARPS), storm-scale numerical weather prediction and data assimilation, *Meteorol. Atmos. Phys.*, *82*, 139–170.
Yu, Z., D. Pollard, and L. Cheng (2006), On continental-scale hydrologic simulations with a coupled hydrologic model, *J. Hydrol.*, *331*(1), 110–124.
Yucel, I., A. Onen, K. Yilmaz, and D. Gochis (2015), Calibration and evaluation of a flood forecasting system: Utility of numerical weather prediction model, data assimilation and satellite-based rainfall, *J. Hydrol.*, *523*, 49–66.
Zabel, F., and W. Mauser (2013), 2-way coupling the hydrological land surface model PROMET with the regional climate model MM5, *Hydrol. Earth Syst. Sci.*, *17*, 1705–1714, doi:10.5194/hess-17-1705-2013.
Zeng, X., and A. Beljaars (2005), A prognostic scheme of sea surface skin temperature for modeling and data assimilation, *Geophys. Res. Lett.*, *32*, L14605, doi:10.1029/2005GL023030.